UNIVERSITÀ
POLITECNICA
DELLE MARCHE

Faculty of Engineering
Course of Biomedical Engineering

Development and Validation of an Ankle Prosthesis Simulator

Candidate:
Enrico Cecchini

Advisor:
Federica Verdini

Coadvisor:
Bernardo Innocenti
Andrea Tigrini

Academic Year 2022-2023

UNIVERSITÀ
POLITECNICA
DELLE MARCHE

Faculty of Engineering
Course of Biomedical Engineering

Development and Validation of an Ankle Prosthesis Simulator

Candidate:
Enrico Cecchini

Advisor:
Federica Verdini

Coadvisor:
Bernardo Innocenti
Andrea Tigrini

Academic Year 2022-2023

Università Politecnica delle Marche
Faculty of Engineering
Course of Biomedical Engineering
Via Brecce Bianche – 60131 Ancona (AN), Italy

Alla vita,
l'amicizia,
l'amore.

Acknowledgments

Ringrazio Bernardo e Edoardo per avermi accolto durante questo tirocinio.

Ringrazio Federica, Andrea e Alessandro per i cosigli dati nella stesura della tesi.

Ringrazio tutti gli amici che mi hanno accompagnato durante questo percorso.

Un ringraziamento speciale a Paolo e Marisa che hanno reso possibile tutto questo.

Santarcangelo di Romagna, 14 Maggio 2023

Enrico Cecchini

Abstract

Injuries and diseases affecting the ankle can cause significant discomfort and hinder regular activities, negatively impacting joint function and movement [1]. Various therapies have been developed to alleviate pain and restore mobility, including total ankle replacement (TAR). The latter aims to substitute the damaged ankle joint with promising long-term outcomes [2]. Moreover, is continuously evolving due to ongoing research, as we can see in the Bologna Oxford TAR (BOX TAR) design [3]. To determine the effectiveness of different prosthetic designs, robotic simulators are commonly utilized to mimic natural ankle joint movements, following the approximations given by ISO 22622:2019, and compare the performance of various prosthetic designs [4].
Thus, the objective of this thesis was to develop a universal robotic simulator that could test both ankle and knee prostheses. In particular, the robot was utilized to assess the effectiveness of a Polylactic acid (PLA) prototype ankle prosthesis during walking.

The robotic simulator utilized in this thesis is composed of four motors, reaching four degrees of freedom, supported by a metallic structure. Two of them allow rotational movements which are Plantar/Dorsiflexion and Internal/External rotation, the third one control the Anterior/Posterior displacement, and the fourth control the Axial load.
Initially, the robot experienced multiple mechanical and electrical problems that had a significant impact on its functionality. In fact, it was unable to move automatically and synchronously, with the axial motor being heavily affected. In particular, three motors could be controlled manually one at a time through their own GUI, while the fourth one (axial motor) wasn't functioning at all.
Nevertheless, the current advanced robotic system can accurately replicate natural ankle movements by executing a variety of synchronous instructions outlined in ISO 22622:2019. These instructions, such as Plantar/Dorsiflexion, Internal/External rotation, Anterior/Posterior displacement, and Axial load, are controlled by a C++ application that was developed as a part of this thesis.

In addition, motors calibration has been performed for controlling the accuracy and precision of the motors. To accomplish this, an Optoelectronic system from OptiTrack was utilized, consisting of three cameras aimed at the motion of three rigid bodies equipped with three markers each. Using this system, the movement of each motor can be precisely measured, enabling the evaluation of motor performance

one at a time. Calibration indicates that only the Internal/External motor has high performance, while the Plantar/Dorsiflexion and Anterior/Posterior motors achieve mediocre performance.

Tekscan 4000 Pressure sensor was used to acquire data on the contact area and force applied between the Tibial and Talar parts of the prototype over two tests. Firstly, comparative research was performed over ten different configurations of the Tibial part, including changes to the Tibial part's position angle with respect to the Transverse Plane of 0°, 6°, and 10° degree and the use of a mobile bearing or fixed bearing. Moreover, from comparative research, the best configuration was found to be a neutral position of 0 degrees with a mobile bearing, showing higher values of the contact area. In fact, this configuration reaches a peak of 373 mm^2 when the maximum load is applied, while the other configurations reach barely 300 mm^2, with the 0 degrees with a fixed bearing reaching 333 mm^2.

Afterward, a repeatability test checked the robot's ability to replicate the same gait cycle multiple times with the same characteristics, seven cycles were performed on the TAR configuration with 0-degree Eversion and mobile bearing. Furthermore, from the repeatability test standard deviation was calculated over cycles, showing good repeatability.

Unfortunately, not all the mechanical problems were solved in particular the Plantar/Dorsiflexion joint and the PLA prototype can't support the total axial load that causes in first place sliding during the test and second the failure of the material due to low compression resistance, for this reason, the axial load applied during testing was halved. Second, the connection between the Internal/External rotation motor and the Axial motor loose grip during the test so the Internal/External rotation was not transmitted to the prototype while testing. However, calibration and repeatability tests confirmed its high accuracy and repeatability, as stated before, confirming the valuable contribution of the study in the field of ankle prosthetics prototyping and testing.

Sommario

Le lesioni e le malattie che colpiscono la caviglia possono causare un notevole disagio e ostacolare le regolari attività, incidendo negativamente sulla funzione articolare e sul movimento [1]. Sono state sviluppate diverse terapie per alleviare il dolore e ripristinare la mobilità, tra cui la sostituzione totale della caviglia (TAR). Quest'ultima mira a sostituire l'articolazione della caviglia danneggiata con risultati promettenti a lungo termine [2]. Inoltre, è in continua evoluzione grazie alla ricerca, come si può vedere nel progetto della TAR Bologna Oxford (BOX TAR) [3].
Per determinare l'efficacia dei diversi progetti protesici, vengono comunemente utilizzati simulatori robotici per imitare i movimenti naturali dell'articolazione della caviglia, seguendo le approssimazioni fornite dalla norma ISO 22622:2019, e confrontare le prestazioni dei vari progetti protesici [4].
L'obiettivo di questa tesi è stato quindi quello di sviluppare un simulatore robotico universale in grado di testare sia le protesi di caviglia che quelle di ginocchio. In particolare, il robot è stato utilizzato per valutare l'efficacia di un prototipo di protesi di caviglia in acido polilattico (PLA) durante la deambulazione.

Il simulatore robotico utilizzato in questa tesi è composto da quattro motori, che raggiungono quattro gradi di libertà, supportati da una struttura metallica. Due di essi consentono i movimenti di rotazione, ovvero la flessione plantare/dorsale e la rotazione interna/esterna, il terzo controlla lo spostamento anteriore/posteriore e il quarto il carico assiale. Inizialmente, il robot ha avuto diversi problemi meccanici ed elettrici che hanno avuto un impatto significativo sulla sua funzionalità. Infatti, non era in grado di muoversi in modo automatico e sincrono, e il motore assiale ne risentiva pesantemente. In particolare, tre motori potevano essere controllati manualmente uno alla volta attraverso la propria GUI, mentre il quarto (il motore assiale) non funzionava affatto.
Tuttavia, l'attuale sistema robotico avanzato è in grado di replicare con precisione i movimenti naturali della caviglia eseguendo una serie di istruzioni sincrone descritte nella norma ISO 22622:2019. Queste istruzioni, come la flessione plantare/dorsale, la rotazione interna/esterna, lo spostamento anteriore/posteriore e il carico assiale, sono controllate da un'applicazione C++ sviluppata nell'ambito di questa tesi.

Inoltre, è stata eseguita la calibrazione dei motori per controllarne la precisione. A tale scopo, è stato utilizzato un sistema optoelettronico di OptiTrack, costituito da tre telecamere puntate sul movimento di tre corpi rigidi dotati di tre marker ciascuno. Con questo sistema è possibile misurare con precisione il movimento di ciascun motore, consentendo di valutarne le prestazioni uno alla volta. La calibrazione

indica che solo il motore Interno/Esterno ha prestazioni elevate, mentre i motori Plantar/Dorsiflexion e Anterior/Posterior raggiungono prestazioni mediocri.

Il sensore di pressione Tekscan 4000 è stato utilizzato per acquisire dati sull'area di contatto e sulla forza applicata tra le parti tibiale e talare del prototipo nel corso di due test. In primo luogo, è stata eseguita una ricerca comparativa su dieci diverse configurazioni della parte tibiale, comprese le modifiche all'angolo di posizione della parte tibiale rispetto al piano trasversale di 0°, 6° e 10° grado e l'uso di un cuscinetto mobile o fisso. Inoltre, dalla ricerca comparativa, la configurazione migliore è risultata essere una posizione neutra di 0° con un cuscinetto mobile, che mostra valori più elevati dell'area di contatto. Infatti, questa configurazione raggiunge un picco di 373 mm^2 quando viene applicato il carico massimo, mentre le altre configurazioni raggiungono appena 300 mm^2, con la posizione di 0 gradi con cuscinetto fisso che raggiunge 333 mm^2.

Successivamente, un test di ripetibilità ha verificato la capacità del robot di replicare più volte lo stesso ciclo di andatura con le stesse caratteristiche; sono stati eseguiti sette cicli sulla configurazione TAR con Eversione di 0 gradi e cuscinetto mobile. Inoltre, dal test di ripetibilità è stata calcolata la deviazione standard sui cicli, dimostrando una buona ripetibilità.

Indipendentemente dall'utilizzo di solo metà del carico assiale specificato nella norma ISO, la parte in PLA stampata in 3D non si è comportata bene durante i test, causando un cedimento dopo un uso prolungato.

Infine, dal test di ripetibilità è stata calcolata la deviazione standard sui cicli, mostrando una buona ripetibilità.

Purtroppo, non tutti i problemi meccanici sono stati risolti, in particolare l'articolazione plantare/dorsiflessione e il prototipo in PLA non sono in grado di sostenere il carico assiale totale che causa in primo luogo lo scivolamento durante il test e in secondo luogo il cedimento del materiale a causa della bassa resistenza alla compressione; per questo motivo, il carico assiale applicato durante il test è stato dimezzato. In secondo luogo, il collegamento tra il motore di rotazione interna/esterna e il motore assiale si è allentato durante la prova, per cui la rotazione interna/esterna non è stata trasmessa al prototipo durante il test. Tuttavia, i test di calibrazione e ripetibilità hanno confermato l'elevata accuratezza e ripetibilità, come già detto, confermando il prezioso contributo dello studio nel campo della prototipazione e del collaudo delle protesi di caviglia.

Contents

List of Figures

List of Tables

Chapter 1

Introduction

Ankle pathologies or traumatic events can have a major influence on the health of the ankle joint and, as a result, the patient's proper locomotion [1]. This can also cause significant discomfort and make everyday living duties difficult. As a result, therapies to alleviate discomfort and restore movement have been developed.

Total ankle replacement (TAR) is a promising and continuously improving treatment. In comparison to knee or hip prostheses, the ankle prosthesis sector is very new, starting in the early '70s by Lord and Marotte [17].

Simulators are widely utilized in the testing and comparison of prostheses. Their purpose is to simulate the joint's natural movement.

The goal of this master's thesis is to continue the work carried out at the Bio-Electro- And Mechanical Systems (BEAMS) department and increase the functionalities of the 4 degrees of freedom simulator for the ankle joint.

The reproduction and simulation of the gait is the major characteristic of this simulator. The latter is composed of four motors supported by a metallic structure, that replicate the rotation and load during gait which are Plantar/Dorsiflexion (P/D), Internal/External rotation (I/E), Anterior/Posterior displacement (A/P), and Axial load.

Initially, the state of the art was that the motors were not able to move in synchro and each motor should be controlled manually through its own GUI, additionally, the axial motor wasn't moving at all. Nowadays, the robot is able to move synchronously all the motors, reproduce complicated tasks such as the gait cycle, and test the prosthesis in multiple situations. Additionally, can be also converted into a knee prosthesis tester, which was its initial purpose.

This report includes the goal of the study, a description of the anatomy of the ankle, an explanation of TAR, a description of the ankle simulator created by the previous projects, the main elements tuned and verified for the present project, and finally a list of improvements that need to be made.

Moreover, the control system is described starting from the C++ application, developed during this thesis for reaching the synchronous movement of the four motors, proceeding with the electrical circuit used for connecting the motors and the PC where the C++ application is running and the creation of the position tables, that are a fundamental tool developed during this internship to deliver commands to

the motors.

Furthermore, a description of the optoelectronic system used for calibrating the motor, and the pressure sensor used to calculate the area of contact and measure a raw estimation of the force applied to the PLA prosthesis.

Finally, the outcomes and planned advancements are discussed.

Chapter 2

Ankle joint anatomy and biomechanics

The ankle joint is a pivotal joint in the human body that plays a crucial role in connecting the lower leg to the foot. It is one of the most intricate joints, characterized by complex anatomy and biomechanics. Its primary function is to enable seamless interaction between the lower extremity and the ground, making it a critical component of the body's weight-bearing system.

Despite the well-established anatomy of the ankle joint, its biomechanics remains a topic of ongoing research. The complexity of its anatomy has a direct impact on its performance, emphasizing the importance of a thorough understanding of its structural and functional features. Thus, before attempting to evaluate the joint's movements and biomechanics, a comprehensive comprehension of its anatomy is crucial.

2.1 Anatomy

The ankle is a hinged synovial joint, created by the interaction of three primary bones [18]. The lower leg consists of two bones, namely the tibia and fibula, while the foot comprises the talus bone. The calcaneus, the largest posterior bone in the foot, is also an essential component of foot anatomy, situated beneath the talus bone. Its anterior section functions as support for the talus bone.

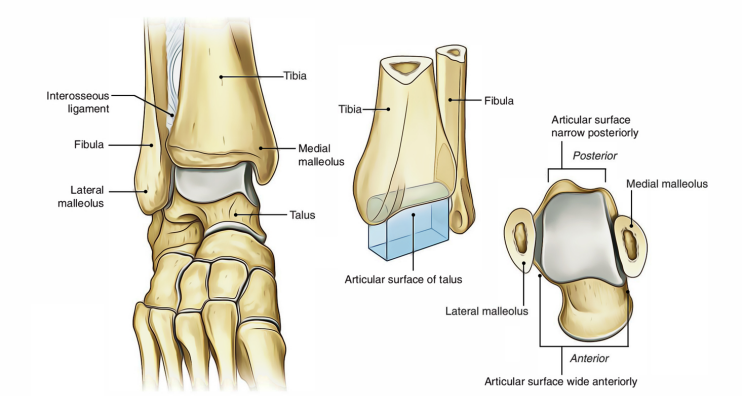

Figure 2.1: Ankle joint and main bones [5]

Although often regarded as a singular joint, the ankle is, in reality, a multifaceted

articulation composed of numerous joints, namely the subtalar joint, tibiotalar joint, and transverse tarsal joint [18]. These three joints are the most significant, and comprehending the ankle's anatomy entails a thorough examination of each of them.

2.1.1 Subtalar joint

At the subtalar joint, as illustrated in Figure 2.2, the talus and calcaneus articulate, forming a synovial joint that is functionally classified as a plane synovial joint.

The joint's movement is primarily limited to eversion and inversion, facilitated by the talus's inferior convex facet interacting with the calcaneus's superior concave facet. While smaller movements are possible, they are restricted.

The joint is supported by multiple ligaments, with the interosseous talocalcaneal ligament being the most critical, connecting the inferior talus facet to the superior calcaneus surface. Additionally, tendons such as the fibularis brevis and fibularis longus contribute to stabilizing the synovial joint [18].

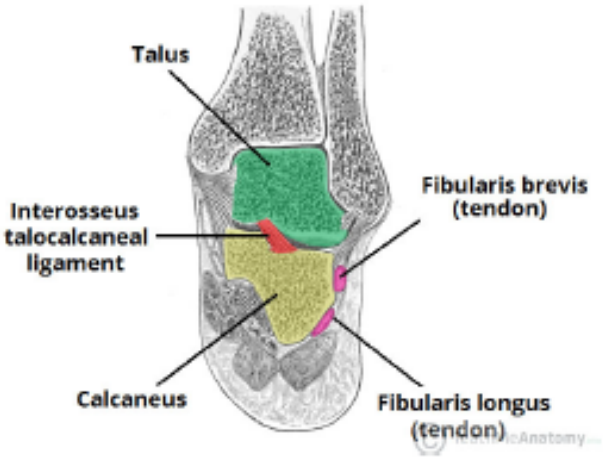

Figure 2.2: Subtalar joint [6]

2.1.2 Tibiotalar joint

The tibiotalar joint is a synovial junction that connects the talus to the distal tibia and fibula, figure 2.3. The trochlea is the superior portion of the talus closest to the lower leg. This is a convex articular surface that fits into the mortise produced by the shine bones' distal portion ends. Furthermore, the talus is constrained by the malleoli of the tibia and fibula, giving him a hinge junction [18].

As a result, the tibiotalar joint is frequently approximated as a simple hinge joint, which is only partially accurate because its flexion is placed at an oblique orientation. The Plantar/Dorsiflexion of the foot is its primary motion. The most secure posture for the joint is dorsiflexion due to the form of the talus, which is broader anteriorly.

Furthermore, the joint structure itself lends stability to the entire complex. It reduces the potential of eversion and valgus strains during everyday activities.

In addition, three major sets of ligaments support the articular capsule. The tibiofibular syndesmosis restricts relative motion between the tibia and fibula, the medial collateral ligaments restrict eversion movements, and the lateral collateral ligaments restrict inversion and rotation. Each of these groupings is made up of numerous smaller ligaments, but that is not the focus of this research. Nonetheless, these are depicted in depth in the figures 2.4a and 2.4b.

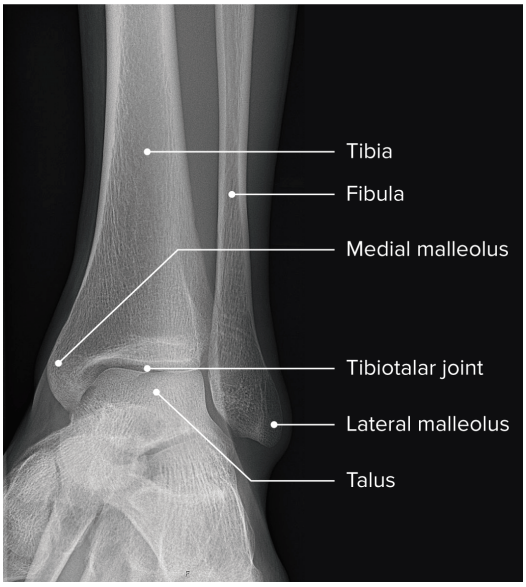

Figure 2.3: Tibiotalar joint [7]

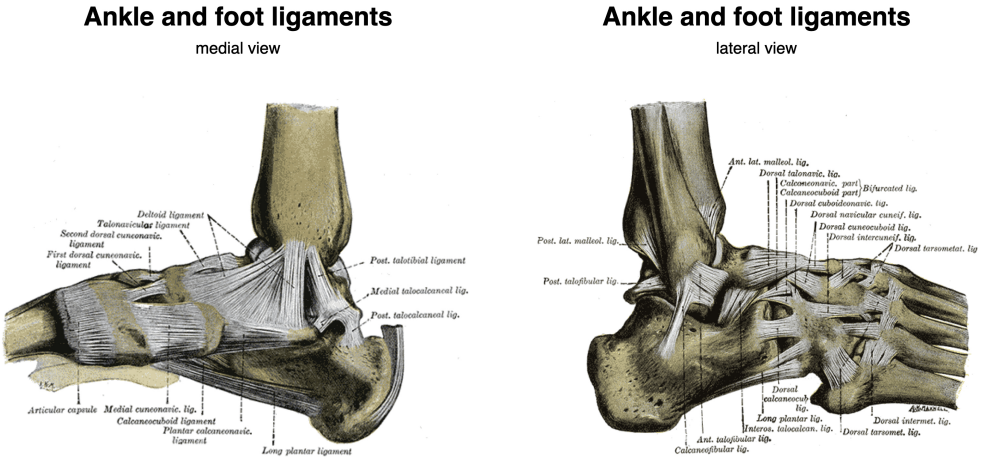

(a) Medial view

(b) Lateral view

Figure 2.4: Ankle and foot ligaments [8]

2.1.3 Transverse-tarsal joint

The transverse-tarsal joint is a compound joint that articulates the hindfoot and midfoot. The talonavicular and calcaneocuboid articulations form two smaller synovial joints, figure 2.5a. The talus and the navicular bone, a tiny tarsal placed proximally to the talus, comprise the first. The calcaneus and cuboid bone make up the second, figure 2.5b.

Moreover, several ligaments will be important in terms of joint stability and flexibility. These two articulations have complicated motions and act simultaneously by fixing one joint while allowing the other to move freely. Supination and pronation of the foot arise from this action. These complex movements involve three motions - adduction, inversion, and plantar flexion - that are antagonistic in nature. Due to their shared axis of rotation, these movements always occur simultaneously. Nonetheless, the primary motion of the transverse-talar joint is still inversion/eversion.

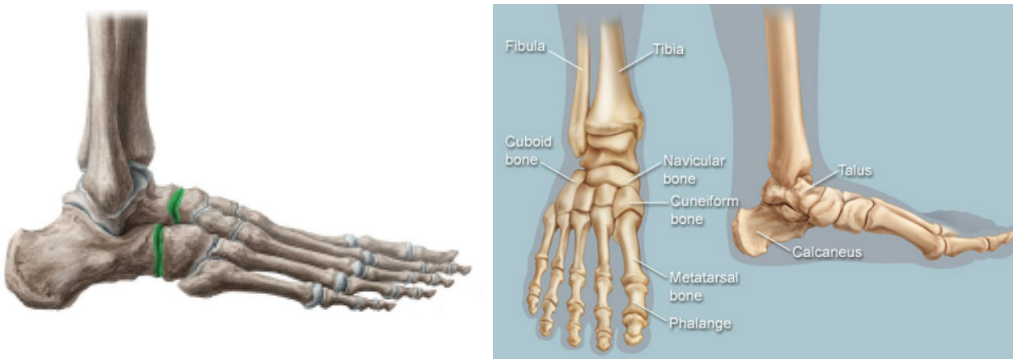

(a) Talonavicular and calcaneocuboid articulations [19]

(b) Ankle joint bones [20]

Figure 2.5: Transverse-tarsal joint

2.1.4 Articular cartilage and Contact area

Ankle cartilage is the thinnest among the joints of the body, ranging from 1 to 1.7 mm, and has a higher compressive modulus [21, 2]. The thinnest cartilage is found in the most congruent joints to help equalize contact stresses [2].

Furthermore, due to its small articular contact surface area (CSA), the ankle joint is subjected to contact stresses of up to five times the body weight during walking [2]. In order to withstand this behavior, under load the talus moves to a position of maximum congruency within the ankle mortise, and fractures or damage to the medial supporting structures can affect ankle congruency. Malunited ankle fractures and other problems can reduce the CSA and alter contact stresses, potentially leading to articular cartilage degeneration and eventual ankle arthritis [2].

Additionally, the CSA was measured with a pressure sensor as reported in [22], and yielded the following values: 229 mm^2, 343 mm^2, 434 mm^2, and 483 mm^2 for

progressive loads starting from 200 N, 500 N, 1000 N, and 1500 N respectively.

Moreover, these anatomical values suggest an increase in contact area related to the enhancement of load during gait. Suggesting that even in the case of a TAR the same behavior is present, in order to understand that comparative research was performed.

2.2 Osteoarthritis

Ankle osteoarthritis is a condition that progressively damages the cartilage of the ankle joint, leading to pain, limited range of motion, and reduced quality of life. Unlike the hip and knee, the ankle joint is seldom affected by primary osteoarthritis. In more than 70% of cases of ankle osteoarthritis, the cause is related to abnormalities in ankle formation or post-traumatic events, typically related to ankle fractures and/or recurrent ankle instability. These abnormalities may result from a single injury or the cumulative effects of multiple sprains [2].

Ankle degenerative joint disease can also be caused by inflammatory arthropathies such as rheumatoid disease, neuropathic arthropathy (Charcot), tumors, or neurological conditions. The variety of potential causes emphasizes the importance of accurate diagnosis and individualized treatment plans to manage ankle osteoarthritis effectively [2].

2.3 Biomechanics

The ankle's biomechanics, like its anatomy, is highly complicated. Furthermore, there is a lot of variation in ankle structure among people. Many factors, including age, gender, prospective illnesses, and so on, might modify the qualities of the joint.

Additionally, joint anatomy has a significant influence on biomechanics, and it is obvious that a connection exists between a joint's structure and its motions.

2.3.1 Ankle motions

Plantar and dorsiflexion in the sagittal plane, eversion and inversion in the frontal plane, and abduction and adduction in the transverse plane are all recognized ankle movements. Moreover, supination and pronation are the names given to the combination of these three actions [9, 18, 23].

The average range of movements for a healthy ankle joint can still be obtained. These data are typically obtained by external analysis using an Optoelectronic system from motion capture, as reported in the next chapter. This implies that appropriately assigning each move to the precise joint might be difficult. The sensors located on the skin are inherently located outside of the joint complex. Nevertheless, it is possible to achieve precise cadaveric measurements, avoiding this problem.

However, these are the literature's average values [9, 18, 23]:

- Plantar flexion/dorsiflexion: the overall range of motion in the sagittal plane is between 65° and 75°. During the stance phase, the range of motion is limited to 25° of which 15° is plantar flexion (PF) and 10° is dorsiflexion (DF). The value in plantar flexion can rise up to 20° during walking.
- Eversion/inversion: range of motion in the frontal plane is approximately 35° (23° inversion 12° eversion)
- Abduction/adduction: range of motion in the transverse plane is around 10° abduction - 20° adduction

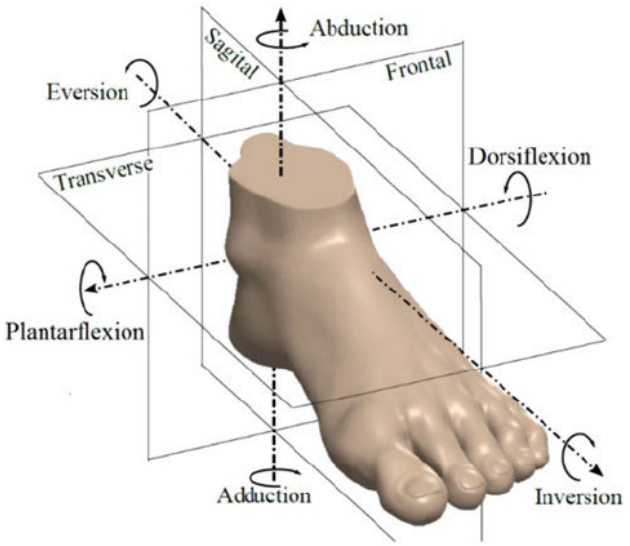

Figure 2.6: Ankle movements and relative planes [9]

Moreover, even while each action happens in a certain plane and ankle flexion is seen as a simple hinge, this is not entirely correct. In practical terms, the tibiotalar joint's axis of rotation is oblique. Dorsiflexion involves a tiny degree of internal rotation. This axis may even vary during motion due to the talus's form, which is not a cylinder but rather a cone [21]. The talus movement of slide and glide is caused by this shift in the center of rotation. This sliding movement cannot be conducted independently of rotation because it is a direct result of it.

2.3.2 Ankle loads and forces

The ankle is the only portion of the body that makes immediate contact with the foot. The obvious result of this is that with any movement, the load is exerted on the ankle joint. This force is primarily applied in two directions: vertical axial load, parallel to the tibial axis, and anterior-posterior force, which is applied to the tibial component in the sagittal plane perpendicular to the axial force axis, as shown in figure 2.7. However, the axial vertical load remains the most relevant direction. This

is the direction of body weight force, and compression occurs mostly along this axis. The anterior-posterior force will cause a little displacement in the joint. Moreover, the amplitude of these loads will be affected by the sort of movement used.

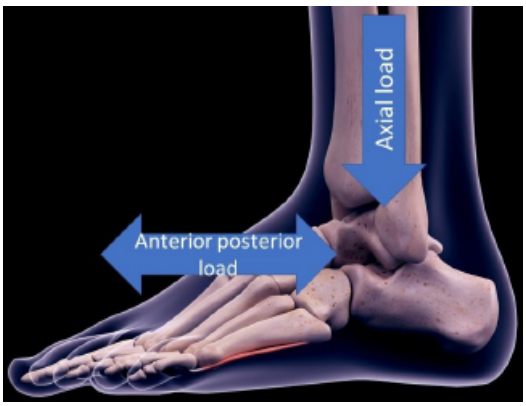

Figure 2.7: Ankle forces [10]

2.4 Giat cycle

The gait cycle refers to the time lapse between successive occurrences of a recurrent event during walking. Usually, it is more practical to use the moment when one foot touches the ground for the first time, also known as "Initial Contact," as the starting point [24].

Walking, being the most commonly observed movement in daily life, is a cyclic motion that can be divided into several stages. Biomechanics research has extensively investigated the gait pattern as it is one of the most studied movements.

2.4.1 Gait analysis

Gait analysis is the systematic measurement, description, and assessment of those quantities that characterize human locomotion, using a set of instruments (such as optoelectronic, electromagnetic, and force platform systems) and anthropometric measurements to acquire kinematic and kinetic data which describes, through a proper analysis, fundamental gait characteristics.

In particular, this analysis is used for identifying biomechanical abnormalities in the gait cycle (GC) that includes quantification as well as interpretation of gait patterns and thus, provides an assessment of human locomotion.

2.4.2 Phases and sub-phases

Gait analysis divides gait into different steps, according to [24].

The major events that occur during the gait cycle are identified using the terms reported below, shown in figure 2.8.

1. Initial contact (IC): the ankle is in a neutral posture, and the heel makes contact with the floor. This sub-phase occurs between 0 % and 2 % of the way through the gait cycle.
2. Opposite toe off (OT):
3. Heel rise (HR):
4. Opposite initial contact (OI):
5. Toe off (TO)
6. Feet adjacent (FA)
7. Tibia vertical (TV) (1. Initial contact).

These events subdivide the gait cycle into seven periods [21], four of which occur in the stance phase when the foot is on the ground, and three in the swing phase, when the foot is moving forward through the air.

In addition, the support phase or contact phase, also called the stance phase, starts with the initial contact and ends with toe-off. Typically, this phase accounts for around 60 % of the gait cycle, resulting in the following time intervals:

1. Loading response (IC-OT): The weight is distributed to the limb. The ankle is plantar flexed at about a 10° angle. This flexion restricts the heel rocker. This subphase occurs between 2 % and 12 % of the way through the gait cycle.
2. Mid-stance (OT-HR): This is the first half of the single limb support procedure. The leg moves forward, and the ankle is in dorsiflexion. This sub-phase occurs between 12 % and 31 % of the way through the gait cycle.
3. Terminal stance (HR-OI): The limb continues to move forward across the forefoot rocker. Dorsiflexion rises and can reach 10°. This sub-phase occurs between 31 % and 50 % of the way through the gait cycle.
4. Pre-swing (OI-TO): The second limb has made touch with the ground. The weight has been withdrawn, and the limb has been unloaded. The heel raises, causing ankle plantar flexion to approach 20°. This sub-phase occurs between 50 % and 60 % of the way through the gait cycle.

While swing phase begins with toe-off and ends with the next initial contact which lasts for about 40% of the gait cycle. It is characterized by the following time intervals:

1. Initial swing (TO-FA): The foot has been elevated off the ground, and the ankle has been slightly dorsiflexed. This sub-phase occurs between 60 % and 73 % of the way through the gait cycle.

2. Mid-swing (FA-TV): The limb moves forward, and the ankle is close to neutral. This sub-phase occurs between 74 % and 87 % of the way through the gait cycle.

3. Terminal swing (TV-IC): The limb progress is finished, but the ankle stays neutral. This sub-phase occurs between 85 % and 100 % of the way through the gait cycle.

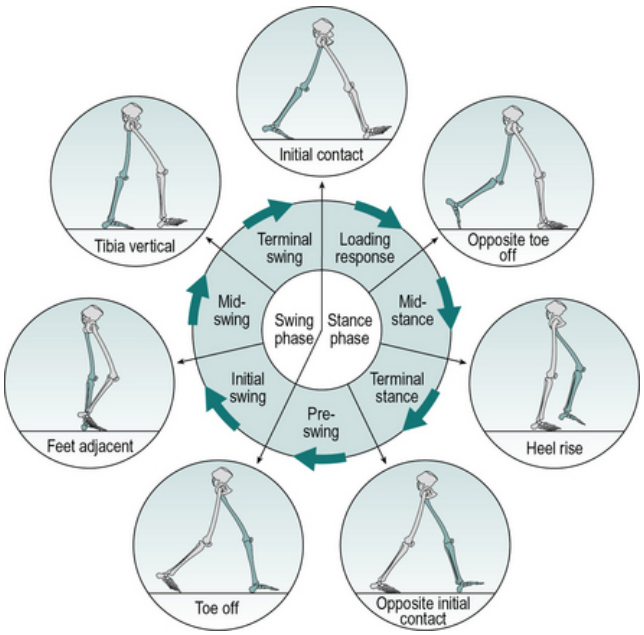

Figure 2.8: Gait Cycle and Phases [11]

2.4.3 Loads

During a typical walk, the average axial strain in the ankle joint is around 4 to 7 times the body weight [21]. The stresses occurring on the ankle joint during distinct sub-phases of the gait cycle may be carefully evaluated. The typical values for a 600N body weight are as follows [18, 21]:

- Initial contact: 675N
- Heel strike: 1350 N
- Midstance: 2100 N
- Forefoot contact: 2550 N
- Push-off: 3000 N
- Toe-off: 300 N

During push-off, the peak value is attained. As previously stated, a value of 3000 N equates to 5 times body weight. The swing phase is irrelevant in this scenario since the reference limb is completely unloaded after the foot leaves the floor.

Moreover, the objective of elderly patients using ankle prostheses is to regain some basic movement. Standing up, walking, and sometimes climbing stairs are the main activities.

The load-bearing area is a metric to consider while evaluating the pressure distribution. The ankle joint's entire load-bearing surface is approximately 11-13 cm^2 [11]. The tibiotalar interface, on the other hand, is approximately $7cm^2$, and this number changes with talus movements. During heel strike and toe-off, this contact region is at its narrowest, while during phases with a high load such as Push-off reaches the maximum value.

2.5 ISO standards requirements and recommendations

As mentioned previously, the aim of this study is to simulate ankle motions in the context of total ankle replacement (TAR), which requires a comprehensive understanding of ankle joint mechanics and the performance of prostheses.

Due to the complexity of ankle biomechanics, it is crucial to refer to reliable sources for guidance. Therefore, the ISO standard is a valuable resource in this regard.

The ISO 22622:2019 standard, titled "*Implants for surgery - Wear of whole ankle joint prosthesis - Loading and displacement parameters for wear-testing machines with load or displacement control and accompanying testing ambient conditions*", is of utmost importance. This document contains a wealth of information regarding ankle prostheses and their testing, including parameters for wear-testing machines and accompanying testing conditions. Moreover, specifies the relative angular movement between articulating components, the pattern of the applied force, speed and duration of testing, sample configuration, and test environment to be used.

In particular, Plantar/Dorsiflexion, Internal/External rotation, Axial load, and Anterior/Posterior displacement are reported as standard values in the ISO standard. For the purpose of this thesis, these values were used for performing a standard test, but these values can be directly yielded from numeric measurements on the patient to test personalized prosthesis.

In this scenario, it is crucial to consider several essential factors, including the durability and wear resistance of the prosthetic materials, the design of the prostheses, the loading and displacement parameters for testing, and the environmental and physiological conditions under which the prostheses will be used. By taking these factors into account, it is possible to develop effective TAR prostheses that can improve the quality of life of individuals with ankle joint pathologies.

Finally, the following points report the main robotic characteristic to respect while testing reported in the ISO:

- The simulator should be inverted with respect to the real situation, the talar component is located above the tibial one.
- The rotational motions are the talar plantar-, dorsiflexion (9 in figure 2.9), and the tibial rotational torque (7 in figure 2.9).
- The contact forces applied are axial vertically on the tibial component (6 in figure 2.9) and anterior-posterior to the interface between tibial and talar components (7 in figure 2.9), simulating normal human walking.

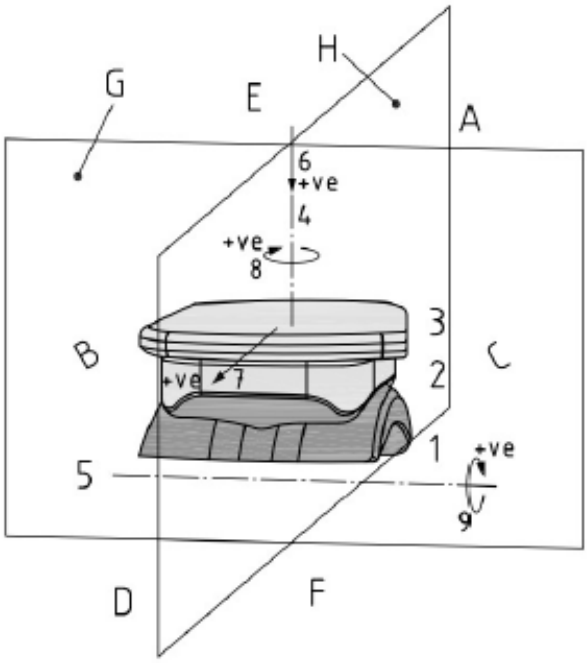

Figure 2.9: ISO representation of the prosthesis

Chapter 3

Total Ankle replacement (TAR)

TAR was developed as an alternative procedure to ankle arthrodesis for advanced ankle osteoarthritis (OA) or traumatic events [2], with the aim of achieving successful development of total hip and knee arthroplasty.

Historically, ankle arthrodesis was considered the gold standard for the treatment of end-stage OA of the ankle joint, as shown in Figure 3.1a. However, long-term follow-up studies of successful ankle arthrodesis revealed that in 44% of patients, especially the elderly, degenerative changes in the hind and midfoot caused disability. Most of these patients required walking aids, and permanent shoe modifications, and had decreased functional ability, as cited in [25].

In view of these limitations, TAR is considered a promising procedure for future treatment to improve the functional ability of the patient [2]. As depicted in Figure 3.1b, TAR offers an effective alternative to ankle arthrodesis for end-stage OA of the ankle joint. The successful development of TAR has opened up new possibilities in joint replacement surgery, thereby expanding the scope of joint arthroplasty.

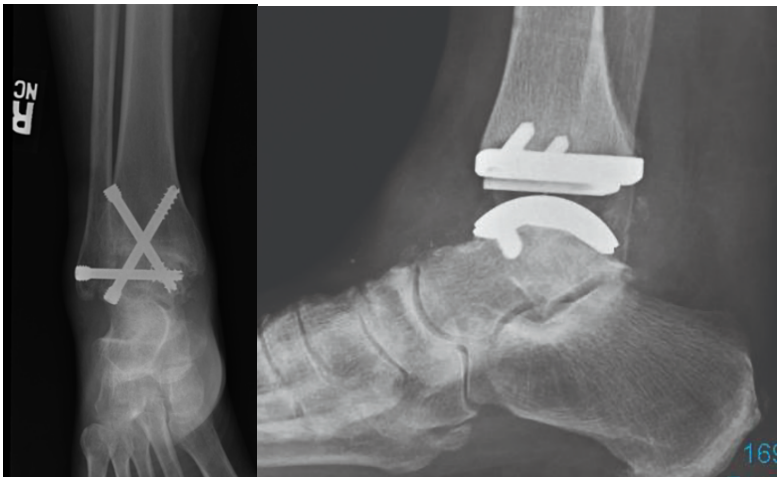

(a) Arthrodesis [26] (b) Total ankle replacement

Figure 3.1: Arthrodesis and TAR [12]

However, achieving favorable outcomes in joint arthroplasty, specifically in ankle replacement, depends heavily on appropriate patient selection. Age, alignment, and

range of motion are critical factors to consider. Total ankle replacement has become a preferred alternative to arthrodesis, providing benefits like joint movement and function preservation. However, certain implants have only shown clinical superiority, and complications such as infections and loosening are major concerns [2].

Successful outcomes from TAR depend on the meeting of specific requirements, such as efficient implantability, which is challenging due to the joint's small size and complex soft tissue, good component fixation for optimal load transfer, correct kinematics compatible with soft tissue complexity, and long-term wear resistance and performance [1]. It is worth noting that not all implant types have demonstrated joint movement and function retention.

3.1 History of TAR

During the 1970s, the first implant was placed by G Lord, J H Marotte, which attempted to replace the ankle joint with a reverse system composed of a ball and socket, where the ball was fixed to the tibia with a stem and the Polyethylene (PE) socket was cemented in the calcaneus [2]. This system had a failure rate of over 50%, and only 28% of patients had satisfactory results at the 10-year follow-up. After that other cemented, 2-component implants were designed but all report a failure rate extremely high in the long term, due to not fully accounting for ankle anatomy [2].

In the 1980s, with the improvement in the understanding of anatomy, material proprieties, and surgical techniques, a new generation of uncemented TAR was designed. It was composed of three parts, two were made of Titanium/Cobalt Chrome (Ti/CoCr) for reconstructing the tibial and talar surfaces. The third part is interposed between the two parts of metal and in this case, was made in PE and fixed to one of the two metal parts. Due to its composition, it was nominated as a two-component, fixed-bearing, such as Agility figure 3.2a, TNK, ESKA figure 3.2b. Moreover, this type of implant, shows high congruency, increasing ankle stability, and reduced degree of freedom, but due to the large interface, torque had early loosening [2].

In the 1990s, to overcome the loosening problem, constraints were minimized, and component congruency was reduced, bringing more mobility in the implant, and higher and more localized stresses [2].

Nowadays, for the design of new implants, an equilibrium between congruence and minimal constraints must be considered. For that reason 3-component mobile bearings were introduced, such as Salto, AES, Hintegra, STAR, BOX figure 4.5, and Buechel-Pappas [2].

3.1.1 Bologna Oxford (BOX) TAR

The model used in this study resembles the Bologna Oxford (BOX) TAR, which is illustrated in figure 3.3. Additionally, figure 3.4 shows the three components of the

(a) Agility TAR [2] (b) ESKA TAR [2]

Figure 3.2: Agility and ESKA TAR

BOX TAR: the Talar part figure 3.4a, Tibial part figure 3.4b, and Mobile bearing figure 3.4c.

The prosthesis's construction is intended to restrict and limit joint mobility in order to maintain the ligaments. It may replicate the original mechanism of the ankle joint, including sliding and rolling action. Clinical studies reveal that after three years, the survival rate is 96 % and the patient stays totally functioning for up to eight years [3]. The prosthesis significantly improves everyday activities such as walking, propulsion, and stair climbing.

Figure 3.3: Bologna-Oxford BOX TAR [13]

The prototype prosthesis used in this thesis is comprised of PLA and is 3D printed. However, the precise prosthesis utilized should not be a big worry because the simulator should be capable of fitting several prostheses. Further chapters will go into detail regarding the simulator's modularity.

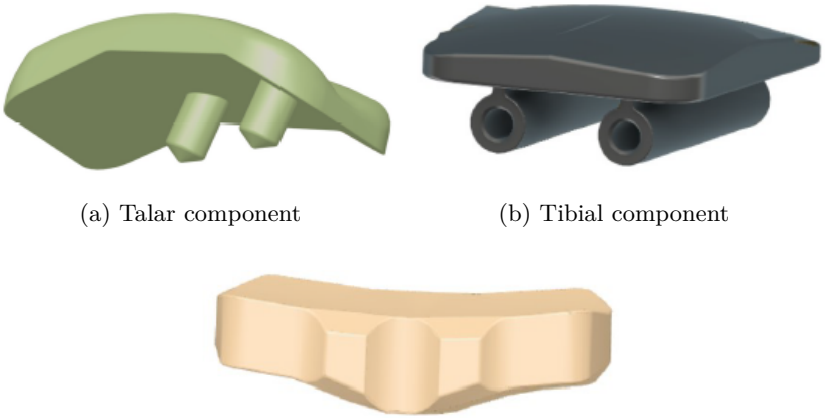

(a) Talar component

(b) Tibial component

(c) Mobile bearing

Figure 3.4: Exploded view of Bologna-Oxford BOX TAR

3.2 Surgery procedure

The success of total ankle replacement surgery depends on several critical factors, such as the correct positioning of prosthetic components, figure 3.5, and the correction of any joint deformities. To enhance the understanding of TAR and its effects on ankle function, recent advancements in instrument-based measurements on radiographs have provided a quantitative assessment of motion and component positioning. This technology has revolutionized the understanding of TAR and allowed surgeons to identify and correct issues that may negatively impact clinical outcomes [27].

In light of this, the current thesis aims to contribute to the growing body of knowledge by analyzing two malpositioned Tibial components and discussing the results in the following paragraphs. The findings of this research will add to the current understanding of TAR and its impact on ankle function. By identifying malpositioned components, this research can help the improvement of surgical techniques and optimize clinical outcomes for patients undergoing TAR surgery.

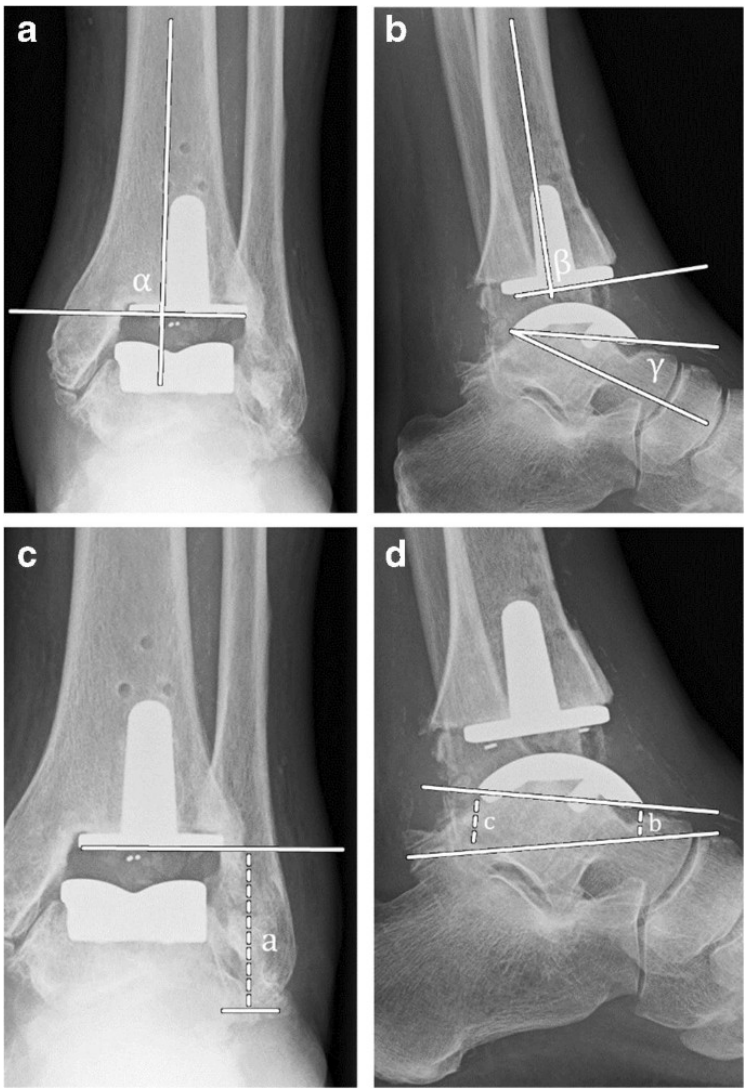

Figure 3.5: Importance of surgical technique [14]

Chapter 4

Robot

The aim of this study is to develop a robotic simulator that can imitate natural ankle movements using multiple actuators. This is done on an ankle prosthesis that is made up of three parts: the talar and tibial components, as well as the moveable bearing that corresponds to the meniscus.

However, the simulator should not be limited to a single prosthesis. The study's ultimate objective is to be able to assess the performance of various prostheses via rapid prototyping. PLA is used to 3D print the prosthetic.

Moreover, force sensors implanted at the interface between the meniscus and the talus should be used to measure the load imparted during the various movements.

4.1 Ankle-foot simulators review

In the literature, two main categories of simulators were identified. The first category involves ankle-foot simulators that are used for in-vitro research on cadaveric specimens, as described in [15]. In certain cases, a prosthesis can be placed on the ankle. This type of simulator is widely used and extensively studied.

The second category involves simulators that are specifically designed for prosthesis research, such as the Ankle/Foot Wear Simulator by Shore Western or the Foot-Ankle Test System by Thelkin. The primary goal in both categories is to simulate ankle movements, with a particular focus on the walking cycle.

4.1.1 In vitro gait simulations

For more than two decades, researchers have had access to in-vitro gait simulations, which have proven to be an invaluable tool for understanding the biomechanics of the foot and ankle [4, 16].

These simulations have benefited from incremental advancements in technology and methodology, such as muscle-tendon actuation, increased degrees of freedom, and advanced control schemes. In-vitro experimentation has allowed for highly repeatable and controlled simulations of gait while measuring various biomechanical signals, such as the muscle activity or tendon resistance [15], figure 4.1, including bone kinematics, intra-articular pressure distribution, and bone strain, making in-

vitro experimentation an important tool for answering clinical questions related to pathology, injury, and surgery [4].

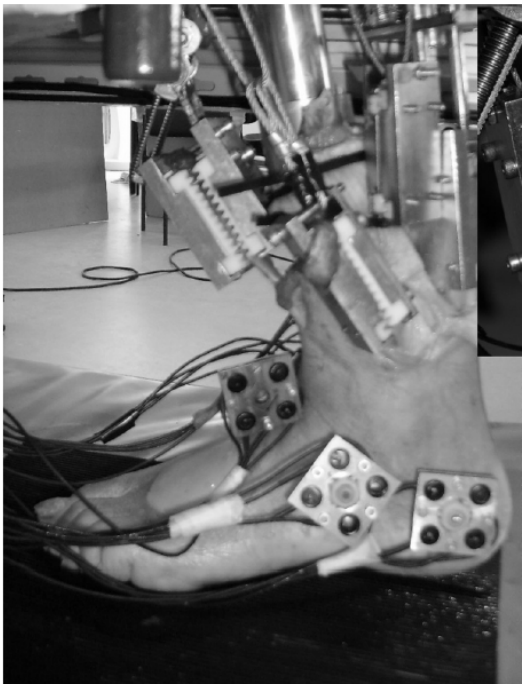

Figure 4.1: In-vitro gait simulations [15]

Moreover, advancements in robotics lead to the possibility of testing human specimens with cutting-edge robots for understanding the performance of different ankle total replacements [28], as shown in figure 4.2.

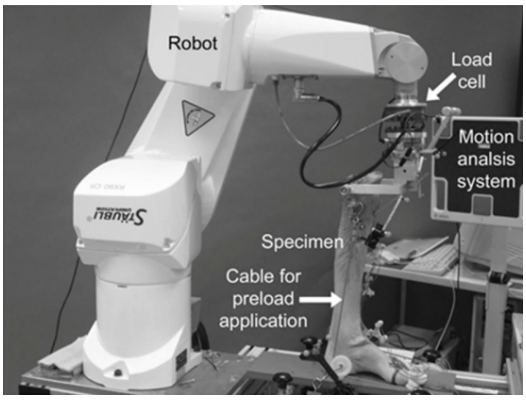

Figure 4.2: Advanced In-vitro gait simulations [16]

4.1.2 Prosthesis testing simulator

There are simulators available on the market specifically designed for ankle prostheses. Both examples discussed below are made for total foot/ankle prostheses, which are

different from the one used in this study, the motions and load profiles should be similar.

Foot-Ankle Test System by THELKIN, figure 4.3a, is a testing system designed for foot and ankle prostheses. The simulator can replicate the walking motion of a leg with varying loads. The system includes a single station with a two-axis load frame for testing the foot and ankle. The system is modular with flexible fixations, allowing for easy mounting of different specimens.

Another example is the Shore Western ankle/footwear simulator, figure 4.3b, which also replicates the walking motion of a leg with corresponding load profiles. This simulator uses a tilting platform that supports the foot, actuated by servo-hydraulic motors.

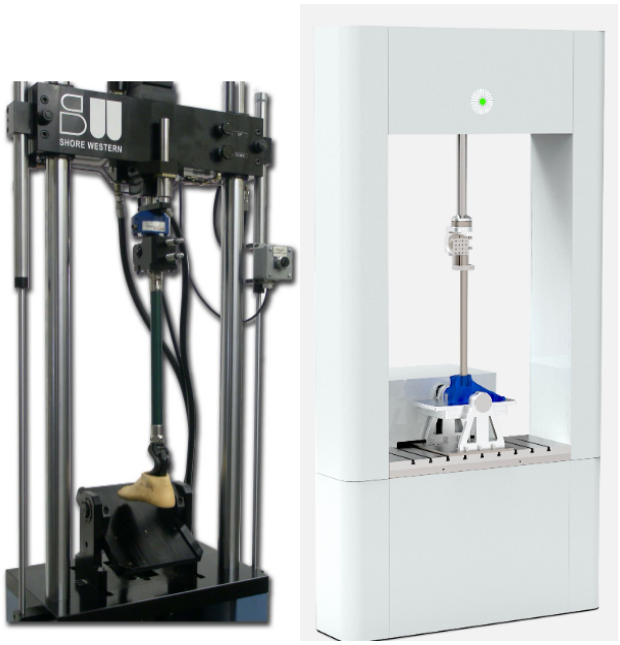

(a) Foot-Ankle Test System by THELKIN [29]

(b) Shore Western ankle/footwear simulator [30]

Figure 4.3: Exploded view of Bologna-Oxford BOX TAR

4.2 Simulator's requirements

First of all, the simulator must follow the values of Plantar/Dorsiflexion, Internal/External rotation, Anterior/Posterior displacement, and Axial Load reported on the ISO.

Moreover, starting from the ISO 22622:2019 requirements and the biomechanics of the ankle during walking, the following requirements can be yielded.

- Plantar- and dorsiflexion must be possible with the simulator. This is the

major motion of the ankle joint and corresponds to a rotation in the sagittal plane. A healthy joint has a range of motion of 65°-75°. However, the amount of range of motion (ROM) required for daily tasks is lowered. Walking allows for a maximum of 30° of plantar flexion and 10° of dorsiflexion [18].

- The simulator must be capable of abduction and adduction action. This is equivalent to a rotation in the transverse plane. A healthy joint has a range of motion of around 30°. During walking, the amplitude is greatly decreased, reaching a maximum of 3° in adduction [11].

- In the range of motion of about 35°, the degree of freedom in the frontal plane should stay unconstrained. This relates to the inversion/eversion motion that might occur during ankle compound motions. This motion will be passively recreated by releasing it. During walking, however, the motion is fairly restricted, with less than 5° amplitude [11]. One the other hand, the ISO standard is not considered so for our purpose is considered equal to zero.

- To accurately imitate real-life events, different amounts of load must be applied. The burden moves in two directions. The vertical axial load along the tibial axis comes first. Second, there is the anterior-posterior force, which is perpendicular to the preceding direction. During walking, the primary direction stays vertical with increased load, up to five times body weight. This figure can be reduced by taking into account lower body weight.

- The ISO standard on ankle prostheses requires that the simulator be inverted with regard to the physiological anatomy. This indicates that the foot is above the tibia. The lower section of the prosthesis is, therefore, the tibial component, whereas the higher part is the talar component.

- Modularity is required for the simulator. By simply swapping out the fixations for the talar and tibial components, different prostheses may be installed on the simulator. This should ideally be quick and simple.

- The framework must be rigid. All parasitic motion must be avoided during simulation or the findings will be skewed. Structures are less prone to vibrations during motions when loads are reduced.

- Motor synchronization is required to conduct complicated motions. Walking is the movement that the simulator must accomplish. Except for the swing phase, the gait cycle must be perfectly emulated. Accessory actions like mounting stairs might be fun to try, but they are not the main focus.

- Pressure sensors are required to measure the area of contact during movements.

4.3 Structure

The frame is made of steel and aluminum, as shown in figure 4.4a, and it holds four motors, two responsible for the rotation and two responsible for the translation/load application, for a total of 4 degrees of freedom. Stepper motors have their own controllers, but linear actuators require a doc circuit, composed of an Arduino and a Maxon 24/2. Other components for synchronizing the motor, including a C++ application, controllers, power supply, and a protoboard, will be discussed in the next section or chapter.

Here is the summary of all the principal component's functions, figure 4.4b:

- Support of the Talar component (number 21)
- Support of the Tibial component (numbers 20 and 5)
- The stepper motor on the top left (number 8) is responsible for the flexion and extension of the ankle, axis y figure 4.4a.
- The stepper motor parallel to the tibial segment (number 16) is responsible for the internal and external rotation of the ankle, axis Z 4.4a. This rotation is transmitted to the tibial component through a belt (number 17).
- The linear actuator in the bottom front (number 14) is responsible for the anterior-posterior force, axis X.
- The linear actuator located below the tibial component (number 18) is responsible for the vertical axial load, axis X.

4.3.1 Motor

As mentioned before, two types of motors have been employed, each having its distinct set of capabilities. Stepper motors are capable of rotating or translating by applying the proper mechanical transformation, while the linear actuator is used for applying loads (axial load).

4.3.2 Stepper motors

Two distinct types of stepper motors have been selected:

- S-SERVO-PR-60L-PG-PN50, figure 4.5, for the flexion/extension motion.
- S-SERVO-PR-60L-PG-PN25 for the internal/external rotation.

The only variation between the two motors is the gear ratio. The first has a 50 gear ratio, as indicated by its name, while the second has a 25 gear ratio.

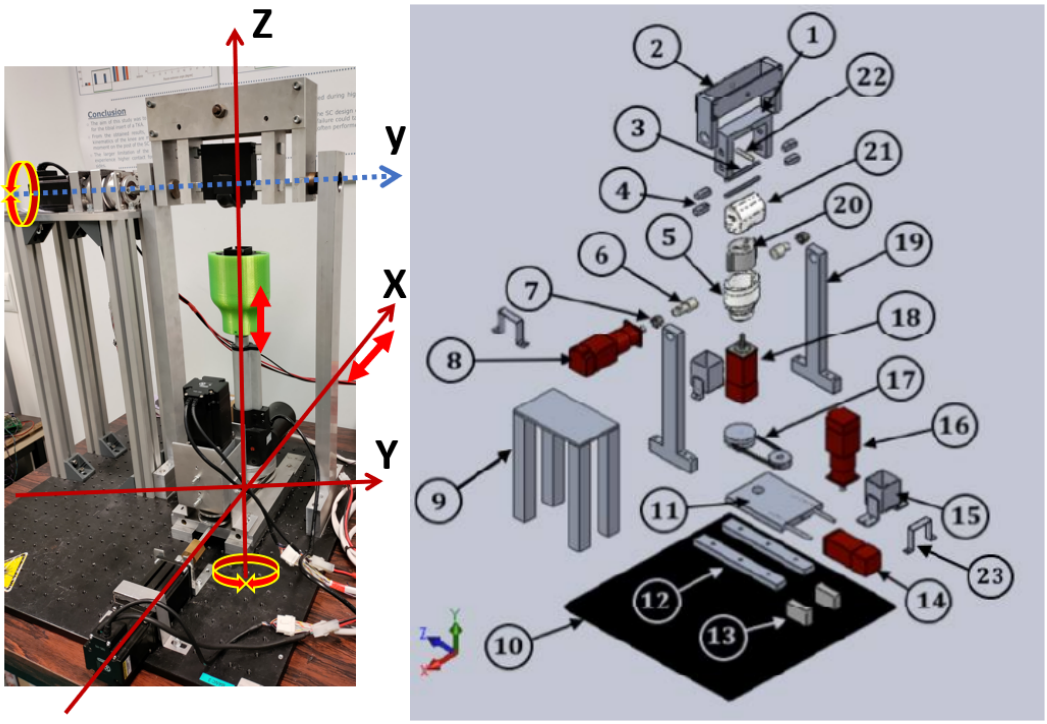

(a) Structure with axis of rotation (b) Structure components

Figure 4.4: Robot structure

Additionally, both motors can be controlled manually or automatically with Ezi-MOTION Plus R v6 software. The most critical parameter that can be modified is the resolution, which is determined by the number of pulses per revolution. The default value of 4000 is chosen, which allows for the calculation of the number of degrees in each step using the following equation [31], resulting in 0.0018 and 0.0036 for 50 gear and 25 gear, respectively, as reported in table 4.1.

$$\frac{Degrees}{Step} = \frac{360°}{Resolution \times GearRatio} \tag{4.1}$$

Furthermore, the significant advantage of stepper motors is that their design allows for zero position inaccuracy. They are also cost-effective, but they require a controller.

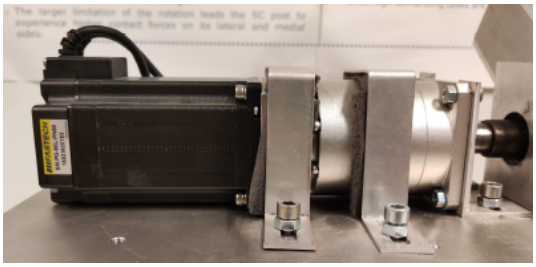

Figure 4.5: Servo Flexion Estention (S-SERVO-PR-60L-PG-PN50)

4.3.3 Linear actuators

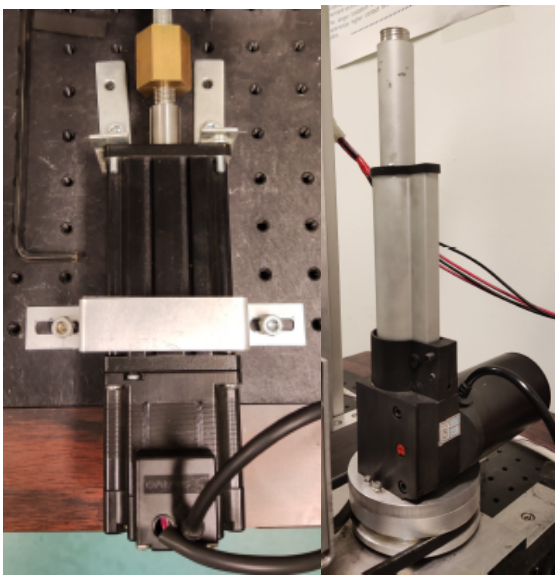

(a) NEMA23C2120A4-200MS, A/P actuator

(b) FD60-24-A8-288.388-C52-HS3, axial load actuator

Figure 4.6: Linear actuators

There are two types of actuators employed:

- NEMA23C2120A4-200MS electro-mechanic actuator is in charge of anterior-posterior displacement. It is, in reality, a stepper motor that enables linear motion by covering rotational motion into translation through a lead screw. This means that it may also be described in terms of stages, as reported in table 4.2, figure 4.6a.
- FD60-24-A8-288.388-C52-HS3 is an electric cylinder that transforms electrical energy into torque via a worm screw, table 4.2, figure 4.6b.

Table 4.1: Rotational motors properties

Motor	Motion in ankle	Gear ratio	Degree/Step	Software used
PN50	Plantar/Dorsiflexion	50	0.0018	Ezi-MOTION
PN25	Tibial Internal/External rotation	25	0.0036	Ezi-MOTION

Table 4.2: Load motors properties

Motor	Motion in ankle	Max load	mm/steps	Software used
NEMA	Anterior Posterior displacement	1200 N	0.00158	Ezi-MOTION
FD60	Axial load	3000 N	/	Arduino

Chapter 5

Control of the motors and synchronization

As previously mentioned in the motor characteristics, the robot is equipped with two distinct types of motors: three stepper motors and one electrical cylinder. It's worth noting that while one of the stepper motors is responsible for translation, this does not impact the control concept.

In order to adhere to the ISO standard for testing, the robot employs two different types of motor control. Specifically, the axial motor is force driven, allowing it to apply the correct level of stress to the prosthesis. Meanwhile, the motors that are controlled with the Ezi-MOTION system are managed for rotations and A/P displacement. Two of these motors are directed by angular displacement to control the Plantarflexion and Dorsiflexion, as well as the Internal and External rotation. The last motor, which is capable of linear displacement, replicates the Anterior Posterior displacement that is reported both in millimeter [mm] and newton [N] in the ISO standard, but for this thesis, the motor is controlled by following the millimeter path.

5.1 Ezi-MOTION

Three of the four motors are controlled by an external controller called Ezi SERVO Plus R, figure 5.1, already present at the beginning of this project. The latter introduces a proportional control loop to control the position of the motors by using the high-precision encoder.

In addition, Fastech offers a graphical user interface (GUI) known as Ezi-MOTION Plus R v6, allowing direct motor operation from a computer without requiring an additional application, enabling the possibility to set up a separate Position Table for each motor, outlining all of the movements that the motor must perform in a sequence. However, this GUI does not allow to achieve synchronization between motors. In order to achieve synchronization using the EziMOTION GUI and control the stepper motor in parallel, a specific connector was purchased, figure 5.2a. As suggested in the previous thesis [31], the circuit in figure 5.2b was realized. Enabling the possibility to send a message to the first motor and trigger in cascade all the motors. Furthermore, for the purpose of this thesis, the circuit reported was reduced by one connector because only three of the four motors work with Ezi Motion.

Figure 5.1: Ezi SERVO Plus R form Fastech

Besides, the previous configuration is not needed if we work directly with the C++ application because in this case each command is delivered separately and sequentially to the motors in order to follow each path specified on the ISO standard in a synchronous way. Moreover, using this application the control scheme of the robot can be represented as in figure 5.3, where each motor has a feedback control delivered by the encoder that is used to monitor the position, speed, and direction of the motor motion.

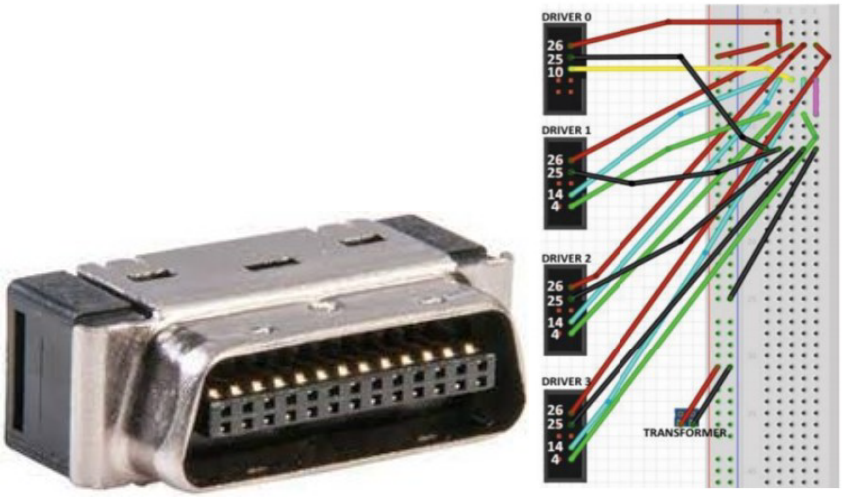

(a) 10126-3000PE connector (b) Electric circuit

Figure 5.2: Synchronization circuit

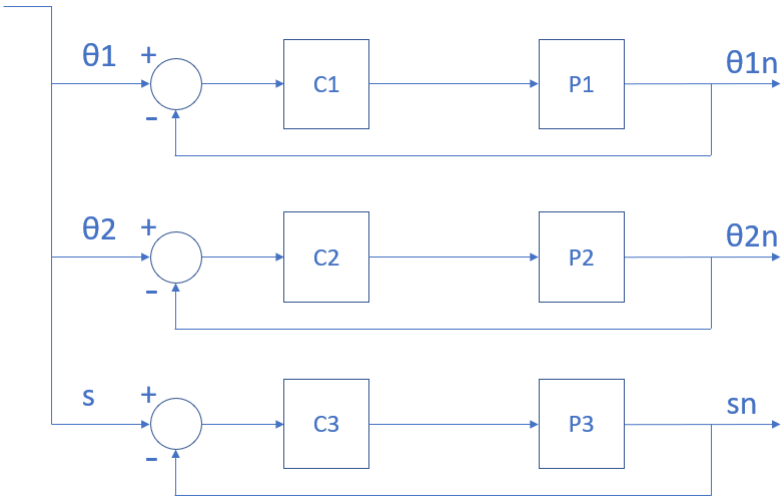

Figure 5.3: Close loop control of Ezi SERVO Plus R form Fastech, present in Internal/External, Anterior/posterior, and Plantar/Dorsifexion motors. Where θ_1, θ_2, and s are the signal of P/D, I/E and A/P respectively sensed by the C++ to the controller C1, C2, and C3. Each controller sends the signal to the corresponding motor P1, P2, and P3. Finally, the movement is detected by an encoder for realizing a feedback control.

5.2 Axial Motor Control

This motor is an electrical cylinder, controlled differently since it requires an external circuit made of an Arduino DUE, figure 5.4a, a Maxon 24/2, figure 5.4b, and a Maxon Motherboard, figure 5.4c. This circuit, in particular, converts the Digital signal, from 0 to 4095, sent by the PC to the Arduino DUE in a Voltage signal, from 0.55 V to 2.75 V, which is then sent to the Maxon 24/2, capable of converting the Voltage signal into an Ampere signal, from -2 A to 2 A, for controlling the force exhorted by the signal, as shown in figure 5.5,[31, 32].

In order to have a perfect conversion from Volt to Ampere the Maxon 24/2 needs to be settled in a specific way through his GUI called EXON Studio as reported in the User Manual and in [32].

5.2.1 Maxon Exon 24/2 setup

Opening the Maxon Studio GUI, the PC is able to automatically detect if a component such as in our case the Maxon 24/2 is connected through a USB/micro USB cable. After this first connection, the setup can start and the user should insert a characteristic parameter that enables the Maxon to have the proper capability and to deliver the right current to the axial motor during the test.

Initially, due to electrical problems in the circuit, the final part of the setup with the GUI, called Auto tuning was not able to deliver the right Amper signal to the motor as shown in figure 5.6a.

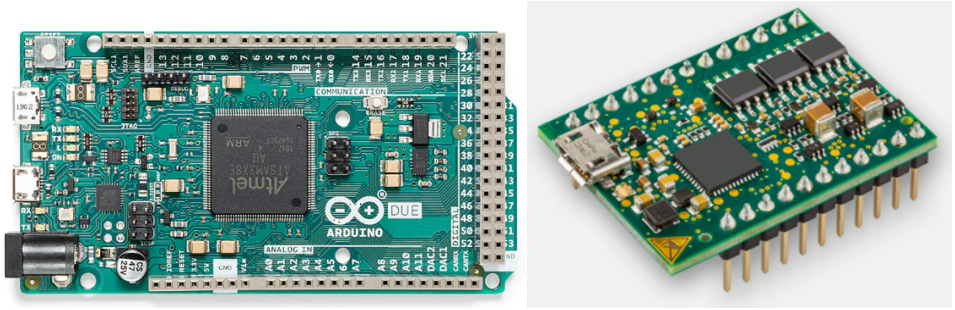

(a) Arduino DUE (b) Maxon 24/2

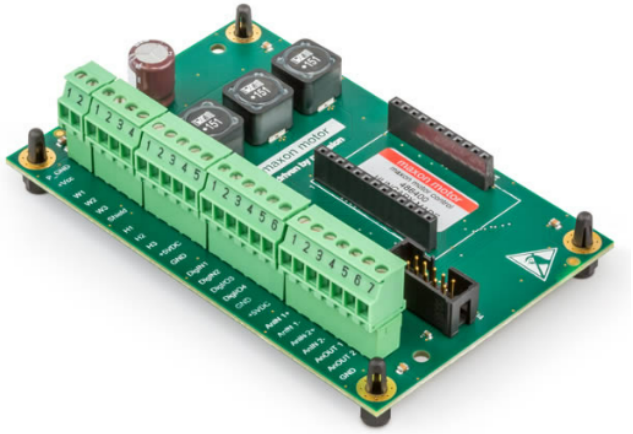

(c) Maxon Motherboard

Figure 5.4: Circuit for controlling the Axial Motor

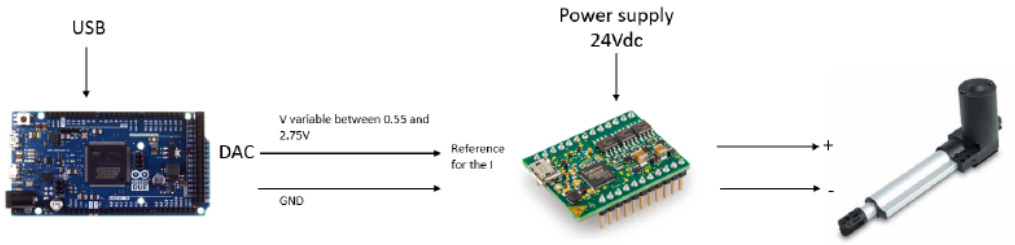

Figure 5.5: Control circuit for the axial motor, composed by the Arduino DUE on the left, the Maxon 24/2 in the middle, and the Axial motor on the right

In fact, by looking at the blue and red lines that are Demand Current and Actual Current in figure 5.6a, the Maxon 24/2 was not able to deliver the Demand Current, in particular, to deliver negative current. This was related to the power supply cables and also to the fact that some cables were broken or partially damaged. So after a proper inspection and substitution, the circuit was able to deliver the right current and move the motor during the Auto tuning and after, as shown in figure 5.6b.

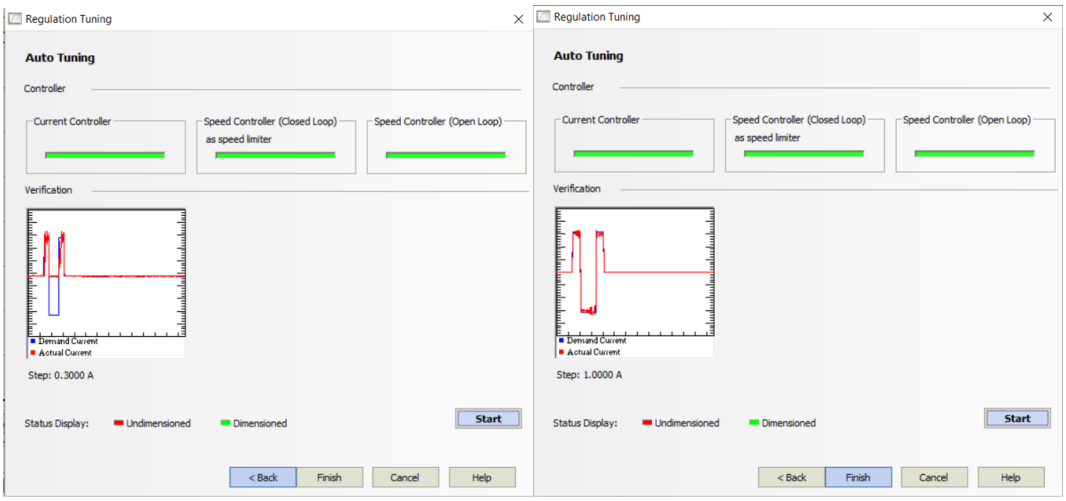

(a) Auto tuning fail (b) Right Auto tuning

Figure 5.6: Auto tuning of Maxon 24/2

Moreover, some values that need to be reported during the setup were not reported by the manufacturer of the motor and so some of them were considered standard. Furthermore, all the values that need to be inserted in the setup are reported step by step in the User Manual in order to have always the same setup and perform the same test with the same characteristics and achieve repeatability.

5.3 Synchronization Code

The primary objective was to synchronize the robotic simulator, which was essential for simulating ankle movements, for this purpose a C++ application was developed during this thesis. In particular, focusing on the simulation of the gait cycle, but the robot is able to replicate other complex tasks such as running and climbing.

Before delving into the synchronization code, several steps were taken, which were not always successful, as detailed below. The synchronization code comprises a primary C++ application and the Arduino code required to convey accurate information to the axial motor.

Initially, comprehending Lobert Marie's C++ code proved to be a primary hurdle due to limited knowledge of the language and insufficient documentation, resulting in a time-consuming process. Despite several efforts, errors were encountered while

attempting to run the program, particularly related to Serial communication and fundamental C++ libraries. As a solution, the program was re-implemented using Python. However, difficulties were encountered while converting EziMOTION standard libraries to Python using PyBind11, mainly due to the presence of binary code in some parts of the libraries, posing a challenge in successfully converting the code. For this reason, a Python code was written to achieve the automation of the EZI Motion GUI.

Finally, a way to get the C++ code working in Visual Studio 2022 has been found, creating an application [App console CLR (.NET Framework)]. By doing that the old functionalities of the code have been restored and drive the motors in relation to a specific position table that the code creates in according to the single position table for each motor written previously by the user.

5.4 Arduino code

This code is used to convert a serial input string into a number, and on the basis of that delivers a Voltage signal to the DAC1 pin, that is then processed by the Maxon 24/2 for delivering the right current to the axial motor. The function is designed to work on an Arduino platform, which is an open-source electronics platform based on simple microcontrollers.

A second Arduino Code was written to control manually the axial motor. The code reads serial input from the computer and performs actions based on the input. The sketch sets up a connection to the computer at a baud rate of 9600. The analog write resolution is set to 12 bits, which means that the analogWrite() function can accept values between 0 and 4095. Pin 2 is configured as an output.

In the loop function, the code checks if there is any serial input available from the computer. If there is, the input is read as a string and stored in the "command" variable. The white spaces around the input are trimmed using the "trim()" function.

However, this second Arduino code is not needed anymore with the introduction of new functions in the C++ application.

5.5 C++ Application

To achieve complete synchronization, the code written by Lobert Marie [31] was revised, with the introduction of new functions, such as [*setorigin*], [*reorderMatrix*], [*scaling*], [*unload*], and [*contact*].

Furthermore, the main functionalities of the code are to convert the position tables stored in the PC into a matrix that contains all the necessary information for driving the motors in a synchronous way. So basically the code is able to produce a new position table containing all the necessary information for controlling the motors. In addition, a for loop was added to perform consecutive cycles.

5.5.1 Funtion; setorigin

The code sets the origin of four motors connected to a serial port with a baud rate of 9600. It starts by checking if the connection to the port is established and if the motor is existent. If the conditions are satisfied, the function sets the origin for each motor in the following sequence Axial motor, Plantar/Dorsiflexion, Internal/External rotation, and Anterior/Posterior displacement.

For each motor, the function first enables the servo, resets any alarm, and moves the motor to position 0. The origin setting of each motor is accomplished by the function '$FAS\_MoveSingleAxisAbsPosEx$' which takes the motor number, position, speed, and other options as arguments. The function outputs the status of each motor after the origin has been set. The system is paused at the end of the function.

5.5.2 Function: reorderMatrix

This code implements a function that sorts a matrix, where the sort is based on a specific column of the matrix. The function takes as arguments a reference to the matrix (matrix) and an integer ('controlColumn') which indicates the column to sort on. Allowing to have a final total position table with always the same order of instruction.

5.5.3 Function: scaling

The "scaling" function takes in a 2D vector of integers called "matrix", an integer called "$control\_column$", and a floating-point number called "$scale\_factor$". The function modifies the contents of the input matrix, allowing it to scale the movement of the robot. In particular, was used to scale the axial load during the test.

5.5.4 Function: Unload

This function unloads the PLA prototype by sending a command over a serial port, first creating a SerialPort object that connects to the COM4 port at a baud rate of 9600. It then prompts the user to confirm whether they want to unload the component by entering 'y' or 'n'. If the user enters 'y', the function sends the character '!' over the serial port to trigger the unloading process. The function assumes that the component at the other end of the serial port is listening for this command and will perform the necessary actions to unload the component.

5.5.5 Function: Contact

The contact function determines if there is contact between the Talar and Tibial parts. It achieves this by creating a new instance of the SerialPort class, which communicates with a device linked to the COM4 serial port, using a baud rate of 9600.

Next, the function prompts the user to input whether the Talar and Tibial parts are in contact or not, with the user expected to provide either a 'y' or 'n' response.

In the event that the user inputs 'n', the function sends a question mark '?' to the serial port. This action initiates positive axial motor movement, resulting in contact between the Talar and Tibial parts, thus enabling the start of the testing process.

5.6 Position Table

The Position Tables are a fundamental tool for the motor's control. In fact, it allows to delivery of multiple commands to perform complex movements such as those required during the gait cycle. Moreover, doc position tables were created during this internship for the control of the motors following the ISO standard.

The Ezi-Motion Gui allows the direct creation of position tables for each motor separately or the import of text files containing the data. Moreover, it was able to have an example of how the position table must be designed in order to give the right commands to the motors, not including the axial one that is controlled with a different electric circuit as reported in the previous paragraph. On the basis of those position tables, we can create our tables respecting the ISO standard using firstly a Matlab code and then a C++ code.

The Position table created for the control of all the motors of the robot is composed of 9 elements as reported in figure 5.7

- noSlv, number of servo.
- p/fIni, initial position for the EZI-motor.
- p/fFin, final position for the EZI-motor.
- dura, time duration of the action.
- absTm, absolute time.
- accTm, acceleration time.
- speed, speed of the movement.
- binIni, initial digital value for Arduino.
- binFin, final position value for Arduino.
- dura, time duration of the action.

The three last elements are present only if we are controlling the axial motor that requires a specific command, that is the conversion of the axial load into the analog input of Arduino.

noSlv	p/fIni	p/fFin	dura	absTm	accTm	speed	binIni	binFin	dura
0	0	2133	500	0	50	7111			
1	0	830	500	0	50	2767.67			
2	0	350	500	0	0	0	2047	2405	0500
3	0	-316	500	0	50	1052.33			
0	2133	616	500	500	50	5055.67			
1	830	861	500	500	50	104.333			
2	350	350	500	500	0	0	2405	2405	0500
3	-316	-3037	500	500	50	9069			
0	616	-2633	500	1000	50	10829			
1	861	855	500	1000	50	19			
2	350	350	500	1000	0	0	2405	2405	0500
3	-3037	-5063	500	1000	50	6752.33			
0	-2633	-5349	500	1500	50	9052.33			
1	855	774	500	1500	50	269			
2	350	350	500	1500	0	0	2405	2405	0500
3	-5063	-5886	500	1500	50	2742.33			

Figure 5.7: Complete Joint Position Table

5.6.1 Position tables creation

In order to achieve the correct cycle for gait a standard sequence of movement is taken into account that follows the ISO 22622:2019 standard. On that basis, different Position Tables were created for each motor. This process was achieved by, first transforming all the values present in the Excel file into float numbers with a Python code (TrasformaMatrici.py), and then the actual position tables were created with a Matlab code (CreatPT.m) that allows the creation of the Excel file from which the position table is copied in a .txt file and adding the file headers, allowing to have the final files that suppose to be taken by the C++ code to give instruction to the motors.

Moreover, in the Matlab code it is possible to change the Acceleration, Deceleration, Speed high and low, and the Waiting time.

5.6.2 Plantar and dorsiflexion table

The Plantar and dorsiflexion table gives instructions to the Plantar/Dorsiflexion motor. As the standard ISO suggests an instruction every second for a total of 100 instructions is given. On that basis, a position table matrix is calculated and given to the motor line by line.

In addition, the position command with a value of zero corresponds to the flexion's neutral value. The Ezi Motion interface allows checking the origin. It is crucial to confirm that the origin matches the neutral value because if it doesn't, the cycle as a whole can be off. Actually, this position was controlled with the information provided by an optoelectronic system as reported in the next chapter, and the Ezi Motion is used to set that value as zero for the motors.

Moreover, the ISO standard gives the values in angle degree (figure 5.8) but that value needs to be transformed in the position of the motor according to the degree/step ratio calculated with respect to the characteristics of the motor (table 4.1).

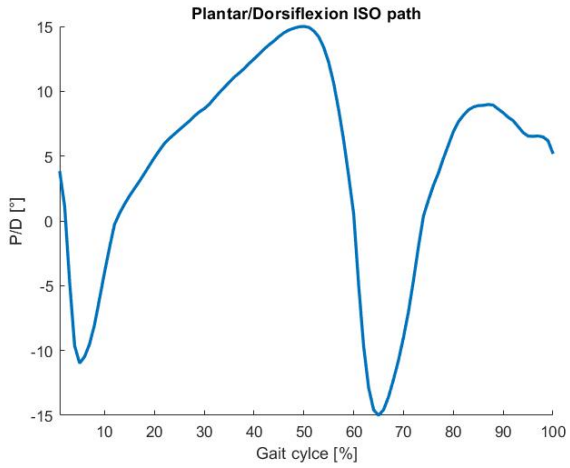

Figure 5.8: Plantar/Dorsiflexion rotation angle during Gait [°]

5.6.3 Internal external rotation table

As for the previous table, also this movement is subdivided into 100 steps that the motor should follow to perform the gait cycle, as shown in figure 5.9.

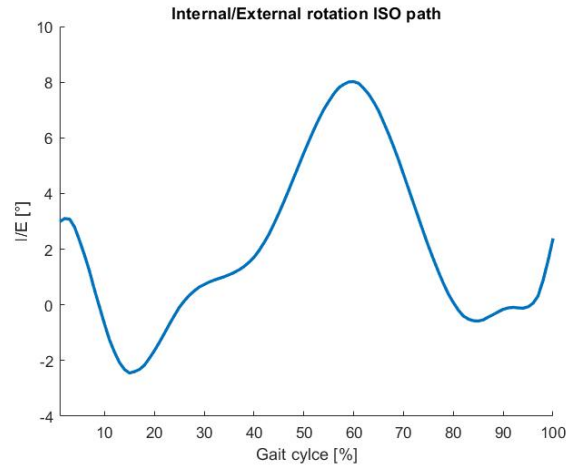

Figure 5.9: Tibial Internal/External rotation angle during Gait [°]

5.6.4 Anterior-posterior table

The ISO standard reports the millimeter values that the movement follows, figure 5.10, so in order to calculate the table we must convert the ISO value into the position of the motor, which is done by considering the ratio that was calculated in the previous thesis (table 4.2).

Moreover, the ISO standard report also the A/P force in newton [N], but for the purpose of this thesis only the A/P displacement was taken into account.

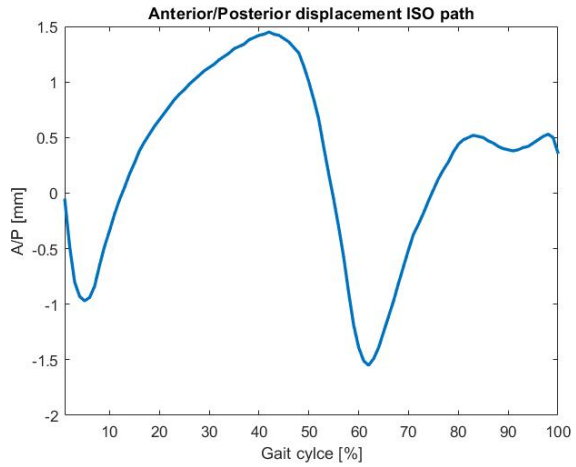

Figure 5.10: Ankle Anterior/Posterior displacement during Gait [mm]

5.6.5 Axial force table

The ISO standard reports the forces that are applied during the gait cycle, figure 5.11, which must be converted by the C++ code in order to have the current necessary to have such force delivered from the motor.

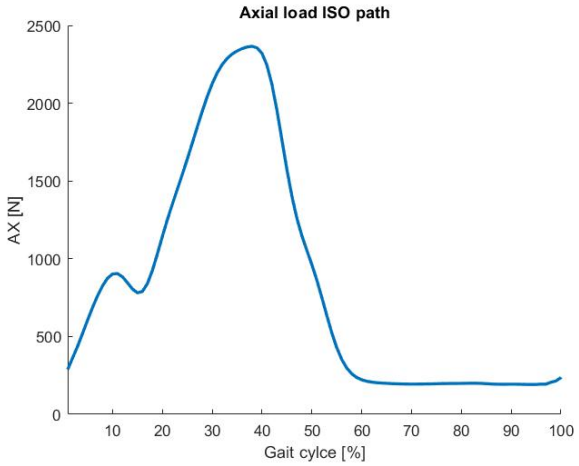

Figure 5.11: Axial Force during Gait [N]

5.6.6 Abduction and adduction movement

The Abduction and Adduction movement is not considered in this robot, even if in the real condition the ankle has a slight movement. But this could be considered in further implementation of the robot, by adding a new motor that performs the tilting around the X axis.

Furthermore, the ISO standard does not consider this movement, but that does not mean that it does not exist.

Chapter 6

Mechanical problems

In order to have a functional simulator and expand the robot's capabilities, various mechanical issues need to be fixed. Starting by drawing new pieces in Solid Works to address this problem, working from a 3D PLA prototype to the final metallic solution, or in some cases directly to the metallic solution.

There were significant mechanical issues with the structure:

- The connection between the Flexion/Extention motor and the Talar component was not stable and new to be renewed in order to have the perfect transmission between the two, as shown in figure 6.1.

- The connection between the Axial motor and the PLA prosthesis was made by an aluminum threaded cylinder that was not able to fix the two components together. So a new metallic threaded cylinder needs to be built, as shown in figure 6.5.

- The connection between the Axial motor and the Anterior Posterior Plate was unstable provoking involuntary movement both in the Anterior-Posterior and Medial Lateral directions. For this reason, a ball bearing (16006 form SKF), figure 6.8, was inserted in the Anterior Posterior Plate to fix the Axial Motor in the Z axis during the movements. In addition, a metallic thrust needs to be inserted in order to avoid any movement of the ball bearing in the case, figure 6.9. Finally, in figure 6.7 the configuration of all parts is shown.

- The transmission belt doesn't have enough grip to rotate the Axial motor when a force higher than 300 N is applied to the PLA prototype. In addition, this force corresponds to the minimum amount of force that is applied to the PLA prototype. In order to solve this problem enlargement of the tensioning mechanism was applied, allowing a better grip on the two pulleys. Still, this method doesn't allow to have a grip able to rotate the motor during compression, so two metallic parts were redesigned to insert a toothed belt, improving the grip. Unfortunately, these two pieces were only designed so can be implemented in the future development of the robot.

  Moreover, also a direct connection between the two motors was designed.

Another possible solution could be a modification in the Code allowing the axial motor to move back each time an internal-external rotation needs to be applied, but this would compromise the performance of the robot in terms of time and most important the ability replicate the gait cycle.

6.1 Flexion Extention joint

The Flexion Extention joint presented instability, making impossible the transmission of the motor movement to the Talar component of the robot. So a new piece was designed in Solid Works in order to improve the connection.

The design of the new piece brings a problem of dimensions, due to the dimensions of the transmission tab, figure 6.2. For this reason, the metal joint was designed with a higher diameter with respect to the old joint. Moreover, this new dimension brings me to: modify also the Lateral support structure by increasing the hole from 28 mm to 32 mm and purchasing a new Needle roller bearing, figure 6.3, for realizing the perfect connection.

In addition to that the Needle roller bearing was chosen firstly due to the lower transversal section with respect to the ball bearing, and secondly high capacity of load and robustness due to the high capacity of load distribution relative to the shape of the volvent components [33].

Furthermore, a cylinder bush is added to the structure as we can see in purple in figure 6.4. This was necessary in order to avoid the direct usury of the lateral support itself and be able when necessary to substitute only the bush and not all the lateral support.

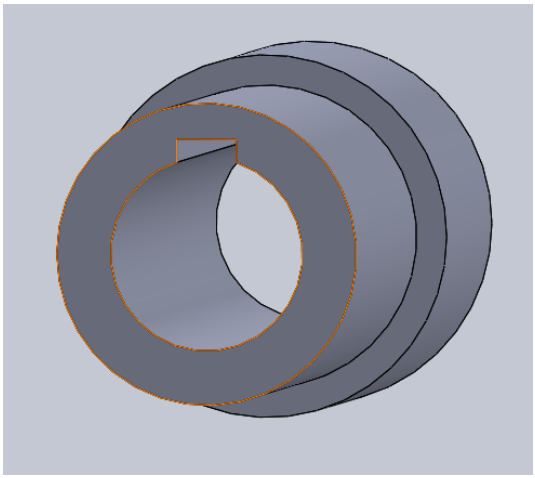

Figure 6.1: Connection between the Flexion Extention motor and the Talar component

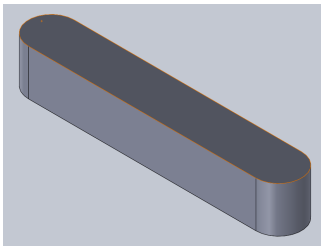

Figure 6.2: Transmission Tab

Figure 6.3: Needle roller bearing, NK 24/20 - SKF

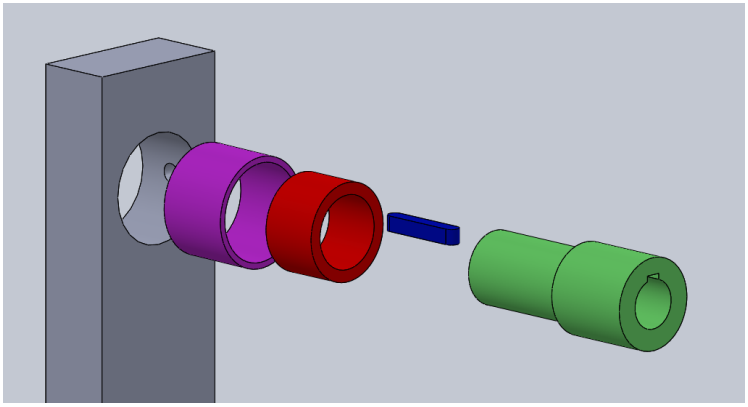

Figure 6.4: In grey we have the Lateral support, in purple the cylindrical bush, in red the Needle roller bearing, in green the F/E joint, and in blue the metallic tab

6.2 Axial Motor - PLA prototype joint

The Metallic Threaded Cylinder, figure 6.5, was designed for respecting the two different filets of the Axial motor and the PLA prototype, to perfectly realize the connection. Moreover, the two fillets were measured with a metric thread, as shown in figure 6.6.

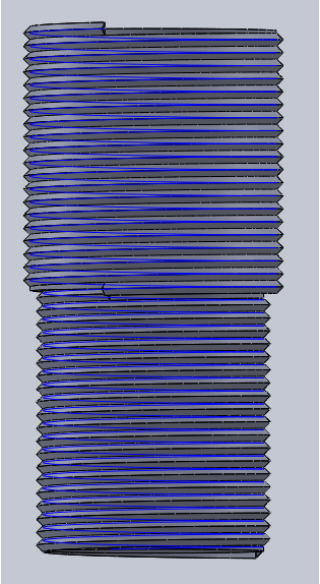

Figure 6.5: Metallic Threaded Cylinder

Figure 6.6: Metric thread

6.3 Axial Motor - Anterior/Posterior Plate joint

Regarding the problem at hand, multiple solutions were considered, including a solution that involves metallic support with a ball bearing allowing for both translation and rotation, which can be fixed in the Anterior/Posterior Plate to keep the axial motor stationary along the Z axis. Various PLA 3D models were designed and printed using a Prusa i3 MK3S for this solution.

Later, an alternative solution was envisioned, as shown in figure 6.7, consisting of the introduction of a Ball Bearing, figure 6.8, a metallic trust to avoid any

displacement during the test of the ball bearing, figure 6.9, and the modification of the Anterior/Posterior plate for the insertion of the ball bearing and 4 holes for fix the metallic trust.

However, the primary goal of this solution was to immobilize the motor and secure it along the Z axis, but this objective is not met with the current solution. Therefore, additional modifications may be necessary. Below some possible solutions are reported.

- Introduce a ball bearing that allows translation and rotation on the mobile cylinder of the axial motor, supported by a metallic structure placed on the Anterior/Posterior plate of the robot.
- Increase the size of the pin of a pulley to 4 cm
- Introduce a new direct connection between the Axial motor and the internal-external rotation motor, as shown in figure 6.10. Moreover, by introducing this direct connection we can avoid making two new toothed pulleys for the Axial motor and the internal-external rotation motor, and deal with the tensioning of the belt.

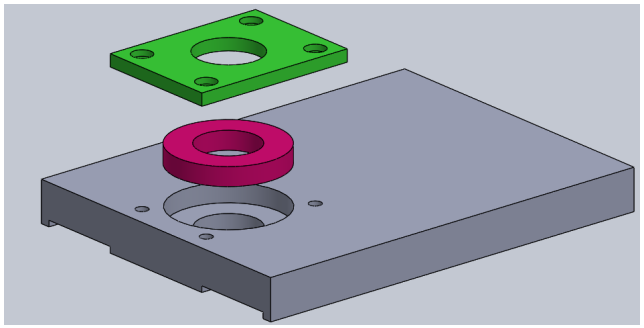

Figure 6.7: In grey we have the A/P plate, in red the ball bearing, and in green the metallic thrust

Figure 6.8: Ball Bearing, 16006 - SKF

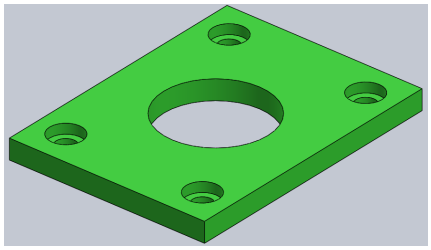

Figure 6.9: Metallic Thrust

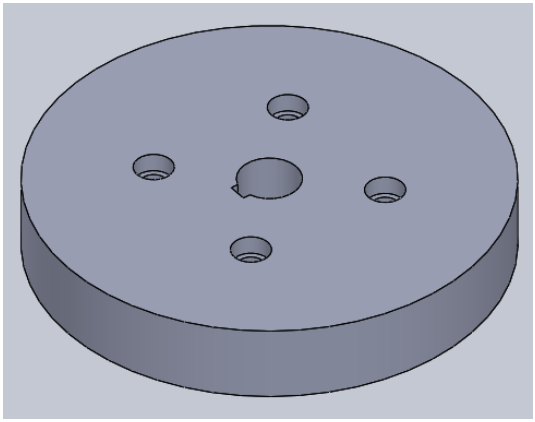

Figure 6.10: Direct connection

Due to the presence of the Metallic Thrust, the support of the abduction adduction motor need to be raised, this was realized by introducing metallic support as shown in figure 6.11.

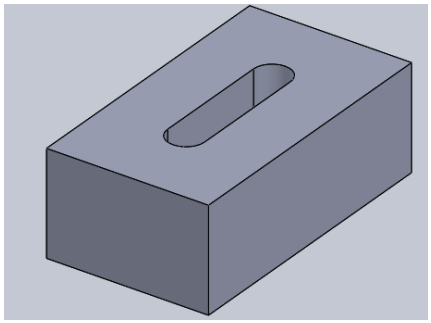

Figure 6.11: Metallic support for the abduction adduction motor

6.4 Transmission belt and tensioning system

To better tension the transmission belt a 3D printed enlargement of the bearing used in the tensioning system was created, as shown in figure 6.12.

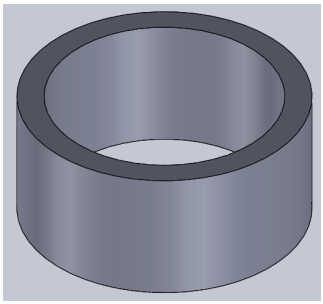

Figure 6.12: Tentioning system enlargment

As previously stated this modification to the tensioning system was not able to give enough grip to the belt, in order to increase the grip and to avoid any loss of friction a toothed belt and pulleys were designed as reported in figure 6.13. Moreover, the previous two pieces were designed for the Metric pitch toothed belt type T5-480-10.

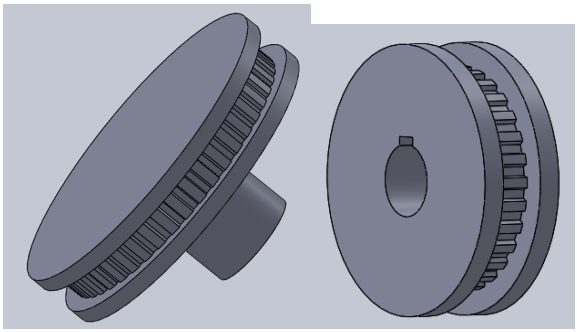

(a) Toothed pulley of the Internal External rotation motor

(b) Toothed pulley of the Axial motor

Figure 6.13: Toothed pulleys

6.5 Metal modeling machine

Machines reported in figure 6.14 and 6.15, are used to make the connection between the F/E motor and the Talar support (figure 6.1).

The Haas Super Mini Mill, shown in Figure 6.16, is a Computerized Numerical Control (CNC) machine that was utilized to modify the Anterior-posterior plate and the Lateral support. This modification was necessary to create the required support for the new ball bearing positioned in the Anterior Posterior Plate.

Figure 6.14: Ageo, Mechanic Press, able to produce a force of 100000 N

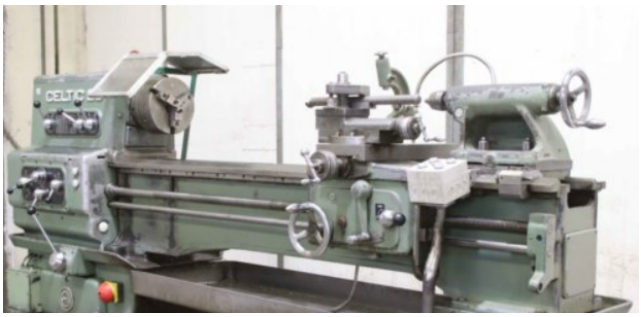

Figure 6.15: Celtic 14, Metal Lathe

Figure 6.16: CNC machine, Haas Super Mini Mill

The CNC machine is capable of performing precise cuts on metal materials, using instructions directly generated by a PC through SolidWorks and a specialized 3D program tool called MasterCAM. MasterCAM enables the creation of the necessary G-code, which can be imported to the machine via a USB memory. With MasterCAM, it is possible to design the path of the cut for the tools to perform the desired modifications.

Prior to cutting, it is essential to calibrate the machine and establish the zero point using a specialized tool that can detect the material and provide the exact position to the PC within the machine.

6.6 3D printing

3D printing is a rapidly evolving technology that has revolutionized manufacturing, prototyping, and design. It allows the creation of three-dimensional objects from a digital model by layering material, typically plastic until the final product is complete. G-code is a programming language used in the 3D printing process to control the movement of the printer's extruder and other components.

This process involves the creation of a digital design of an object using computer-aided design (Solidworks or CAD) software. This design is then used to produce a physical object layer by layer through an additive manufacturing process. The 3D printing process can be used for various applications, including creating prototypes, custom parts, and even replacement organs.

For the purpose of this project a Prusa i3 MK3s was used, figure 6.17a.

6.6.1 G-code

G-code is a programming language used to control the movement of the 3D printer's extruder and other components, figure 6.17b. It is a standardized language that has been adopted by most 3D printing software and hardware manufacturers. The G-code tells the printer how fast to move, how much material to extrude, and where to place the extruder head.

G-code is critical to the 3D printing process because it controls the printer's movement and ultimately determines the final product's quality. Without G-code, the printer would not know where to move, how much material to extrude, and how fast to move. The G-code also provides a level of customization and flexibility in the printing process, allowing designers to create complex shapes and structures. In this thesis, the G-code was automatically generated by the PrusaSlicer GUI developed by Prusa, figure 6.17c.

(a) 3D printer

```
434760 G1 F1500
434761 G1 X129.453 Y124.073 E.77282
434762 G1 X129.453 Y120.686 E.11463
434763 G1 X143.473 Y106.667 E.67113
434764 G1 X144.415 Y105.842 E.0424
434765 G1 X145.451 Y105.149 E.04216
434766 G1 X146.637 Y104.56 E.04483
434767 G1 X147.873 Y104.144 E.04415
434768 G1 X149.09 Y103.903 E.04201
434769 G1 X150.361 Y103.818 E.04311
434770 G1 X178.005 Y103.818 E.93571
434771 G1 X178.005 Y106.368 E.08631
434772 G1 X163.205 Y106.37 E.50096
434773 G1 X146.194 Y108.371 E.57977
434774 G1 X146.133 Y108.4 E.00229
```

(b) G-code generated by PrusaSlicer

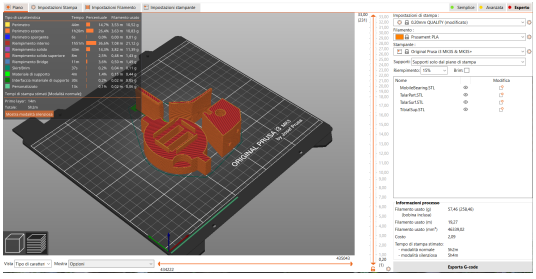

(c) PrusaSlicer

Figure 6.17: 3D printer Prusa and his native GUI

Chapter 7

Optoelectronic system

Optoelectronic systems are methods of motion analysis based on image acquisition via video cameras. For the purpose of this thesis a system of three cameras where utilized to capture the movement of three rigid bodies for measuring the movement of the motor.

7.1 Passive Markers

Movement analysis involves the use of one or more cameras, markers, and marker's support, figure 7.2a,7.1a,7.1b respectively.

Markers are spherical or hemispherical objects able to reflect infrared light transmitted by the cameras, used to facilitate their recognition by the instrumentation and their application on the subject to be studied. The latter are fundamental objects in the study of movement in the laboratory, as they make it possible to determine the position of points of a body in space.

In order to perform motion capture, 3 rigid structures were 3D printed, figure 7.1. The arms of this structure have different lengths, on top of each arm the passive markers are placed, in order to define 3 different rigid bodies with the optoelectronic system and enable the detection of angles and movements in the detection space of the cameras.

7.2 Camera Calibration

Calibration, the determination of the geometric parameters governing the three-dimensional system in use, is one of the fundamental steps in the determination and study of motion in the laboratory. Without it, it would not be possible to estimate the exact position of a point with respect to the reference system used.

There are, in fact, various distortion factors that cause errors in the acquisition, but on the other hand, there are just as many calibration parameters that can be classified into two subgroups:

- Internal parameters: parameters directly linked to the structural characteristics of the cameras used for filming, which are: focal length, reference point coordinates, and distortion coefficient.

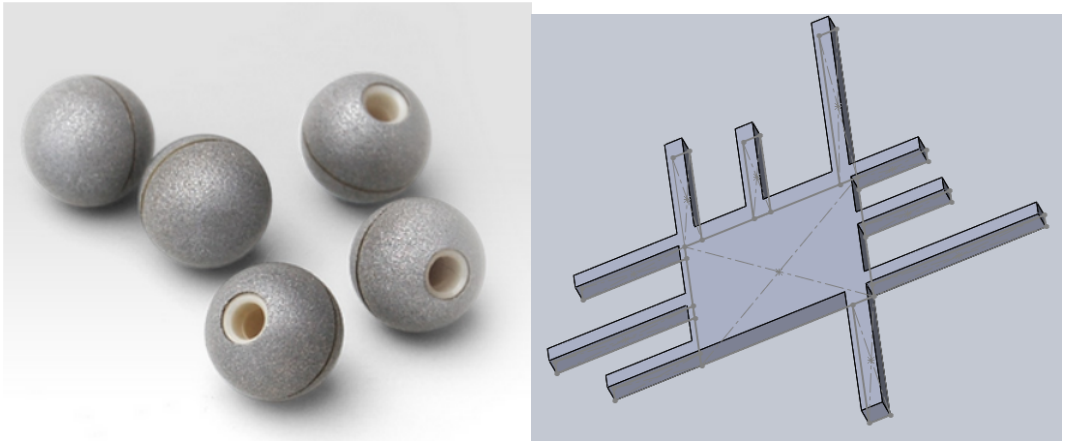

(a) Passive Markers (b) Marker's support

Figure 7.1: Marker and support

- External parameters: related to the characteristics of the laboratory and the positioning of the various cameras such as the position of the camera reference system with respect to the absolute reference system.

It is therefore clear that if a camera is moved, the internal parameters are not changed, but rather the external parameters of the system, whereas if the optics and assembly are changed, the internal parameters vary.

In practice, the determination of these parameters leads to the definition of a roto-translation matrix M that relates the absolute reference system (of the laboratory) to the reference system of the cameras that correspond to the center of the lens.

7.3 Tracking

Once you have all the cameras calibrated, you proceed to reconstruct the movement of the markers in space. It is necessary to have at least two camera points to reconstruct a 3D point of the marker. The points of interest for this phase are the coordinates of the projections in the image plane reference system (x,y) (i.e. the coordinates inherent in the images of the cameras that are filming the marker) and the coordinates of the marker in space (x,y,z).

For this thesis, the motion capture system was composed of three cameras, so in order to reconstruct the position of a marker during the test, three sets of planar coordinates were taken into account.

7.4 Optitrack

OptiTrack provides high-performance optical tracking at the lowest costs in the sector, such as high-speed tracking cameras, and motion capture software.

Allowing the use of this system in different fields of industries, including film and gaming, sports training, and biomechanics.

7.4.1 High-speed tracking cameras and PC connection

The system setup for the acquisition of the motion data in this thesis is composed of three Camera Optitrack Flex 3, figure 7.2a, positioned in 3 different angulations with respect to the Robot in order to be able to detect the movement of the Rigid Bodies during the tests.

All the cameras are connected to the same hub, figure 7.2b, with a USB 2.0 cable to achieve frame synchronization and transmit data to the PC. Furthermore, data were acquired with a velocity of 100 Frame Per Second (FPS).

(a) Camera Optitrack Flex 3 (b) Optitrack OPTIHUB

Figure 7.2: Camera and synchronization system

7.4.2 Optitrack GUI: MOTIVE

Motive is the graphical computer interface that Optitrack gives in order to calibrate cameras, define rigid bodies, and manage motion detection data.

The calibration is performed with a special wand, figure 7.3, which is a standard length and where 3 markers are positioned in standard positions known a priori. The wand must be moved in all the 3D spaces that need to be detected and in automatic, the software is able to store the position data and performed the calibration of the space. In order to do that a minimum amount of points in the space of detection must be acquired (at least 2000 points per camera were taken), figure 7.4, to allow the software to position all the cameras in the virtual space and fix their global position with respect to the reference system.

After the calibration, we can insert the markers in the cubic volume and the cameras are able to define their position, figure 7.5, allowing us to define rigid bodies by selecting 3 markers in the same support.

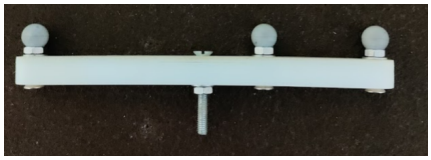

Figure 7.3: Calibration Wand

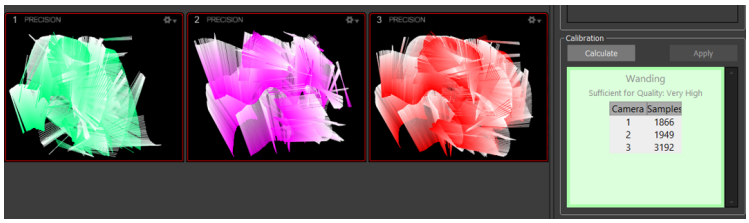

Figure 7.4: Calibration of the cameras

Finally, we are able to detect the movement of rigid bodies. So data are acquired and used to calibrate the movement of the motor.

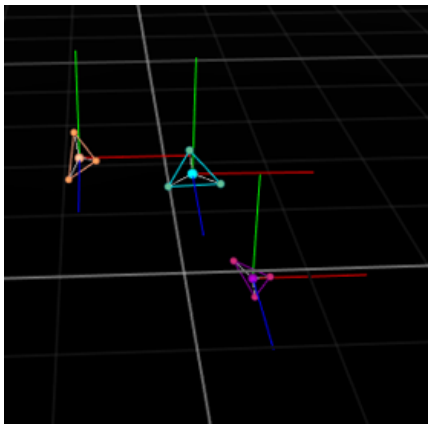

Figure 7.5: Rigid bodies definition into Motive environment

7.5 Motor Calibration data acquisition

Motor calibration was a fundamental step in order to understand the real performances of the motors.

The movement of each motor was detected by 3 cameras, and 3 marker supports were attached to the robot, in particular with the following scheme, two on the metal frame as reference points and the third one on the motor that performs the movement, as shown in figure 7.6 for Plantar/Dorsiflexion motor. Furthermore, as shown in figure 7.6, during these acquisitions the reference frame was considered as follows: Plantar/Dorsiflexion is around x axis, Internal/Eternal rotation is around Y axis, and Anterior/Posterior displacement is along Z axis as reported in table 7.1.

Marker support is composed of 3 markers, this configuration allows the definition

Table 7.1: Data extracted with Matlab for the Optoelectronic system Excel files

Plantar/Dorsiflextion [°]	Rotation X (Pitch) RB1
Internal/External rotation [°]	Rotation Y (Yaw) RB3
Anterior/Posterior displacement [mm]	Position Z RB3

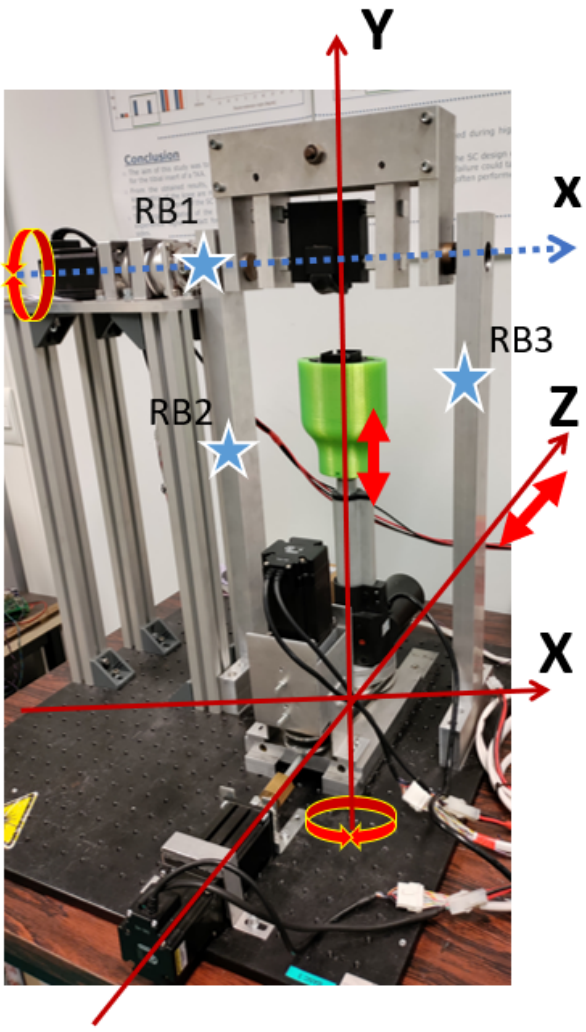

Figure 7.6: Rigid bodies disposition during the calibration of Plantar/Dorsiflexion motor

of 3 rigid bodies (RB), which are the minimum amount of data for extracting the Plantar/Dorsiflextion angle, the Internal External rotation angle, and the Anterior Posterior displacement, during different acquisition.

Firstly the data were acquired during the overall simulation of gait, but this influenced the detection of the movements causing errors in the measurement, so a second take is performed by acquiring each movement separately one motor at a time with the previously explained markers disposition.

Additionally, in order to calibrate and measure the accuracy of each motor, the movement was acquired five times with a total of 15 trials, but due to systematic error related to a failure in data transmission Camera-PC, some trials were discarded.

Finally, data were exported from the Motive GUI in the form of an Excel file, and useful data were extracted using a MatLab code. From each acquisition different motions were extracted, which are:

- Rotation of rigid body 1 in X for P/D. For this acquisition marker supports were displaced two on the metal frame and Rigid Body 1 on the axis of rotation of the P/D motor.
- Rotation of rigid body 3 in Y for I/E. In this case, the marker supports were displaced two on the metal frame and Rigid Body 3 on the axis of rotation of the I/E motor.
- Position of rigid body 3 with respect to the other rigid bodies in Z of A/P displacement. Marker supports were displaced, two on the metal frame and Rigid Body 3 on the A/P plate.

Moreover, this code was used for data visualization, in order to understand if the movement of the motors correspond to the actual standard suggested by the ISO tables. The result of this calibration will be reported in the Result chapter.

Chapter 8

Pressure sensor

Understanding how the load is applied to the surface of the PLA prosthesis is possible by applying a load sensor between the two contact surfaces. This allows us to have a diagram of the force during time and also to measure the area of contact between the Talar part and the Tibial part of the robot, which are parameters useful for evaluating the performance of the prosthesis.

Different typologies of sensors were present in the laboratory, so a selection has been made on the basis of the technical specifications required, such as the sensor dimensions, sensitivity, and spatial resolution. Finally, Tekscan 4000 was selected, figure 8.1. The latter is specifically designed for biomechanics applications, the flexible sensor utilizes piezoresistive technology to measure the force and contact area of two surfaces [34]. The Evolution 2 by Tekscan is used to connect the pressure sensor to the PC, allowing for the acquisition of data and real-time display, as shown in figure 8.5.

Table 8.1: Tekscan Pressure sensor 4000, data sheet specifications. Where MW is Matrix Width, MH is Matrix Height, CW is Column Width, and RW is Row Spacing, as shown in figure 8.1

MW	MH	CW	RW	N. of Sensel	Spatial resolution [Sensel per cm^2]
27.8 mm	33.0 mm	0.8 mm	1.0 mm	572	62.0

8.1 Sensor arrangement

The sensor's sensing area comprises two rectangles measuring 27.9 x 33.0 mm (MW x MH), with a spatial resolution of 62 Sensel per cm^2, as indicated in table 8.1 [35].

Thank to the flexibility of the sensor, a specific arrangement of the sensor was used, connecting the two parts of the sensor one after the other, in order to have a wide area of sensing, 18,41 cm^2, distributed under the Talar part of the robot, as shown in figure 8.2.

This allows calculating the area of contact over firstly on the gait cycle and on some modifications on it such as double Plantar/Dorsiflexion. This second configuration was taken into account only for evaluating the critical point of the robot for future

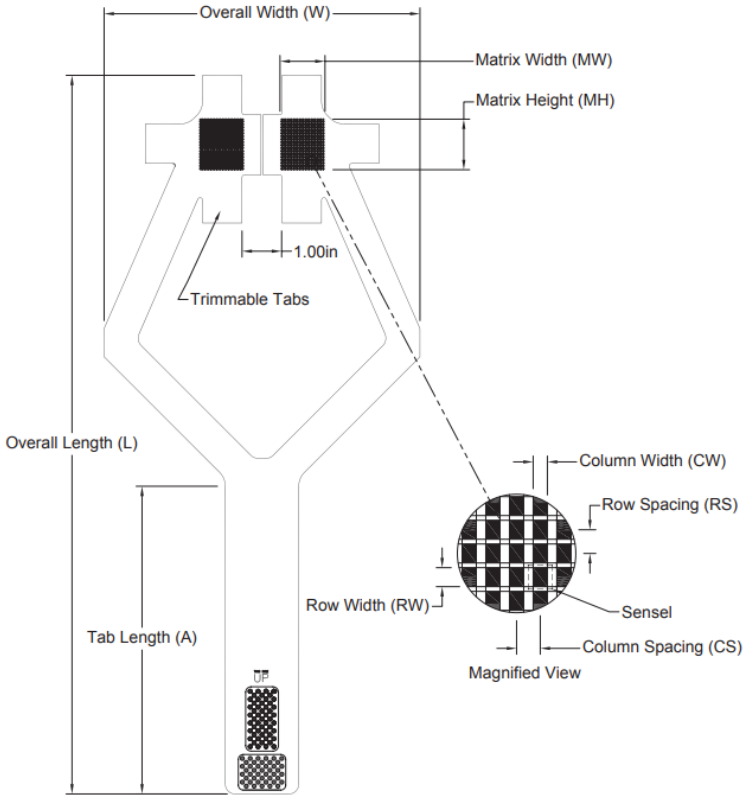

Figure 8.1: Pressure Mapping Sensor 4000

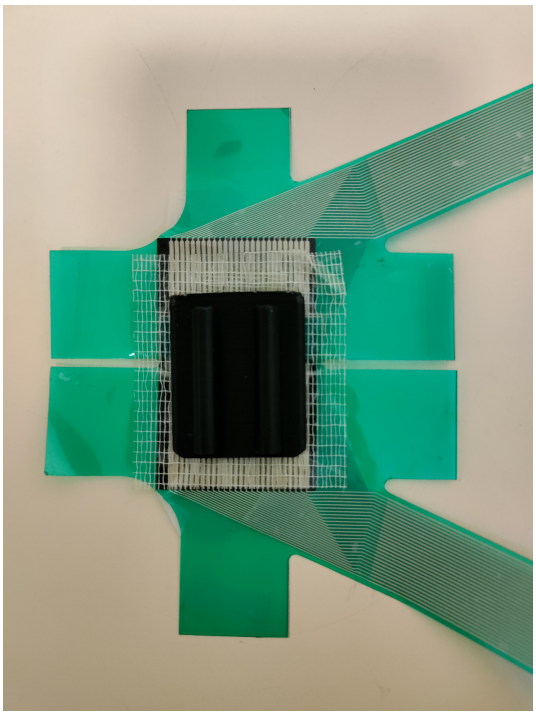

Figure 8.2: Sensor disposition for increasing the sensible area

testing, so the data acquired were not analyzed to evaluate the performance of the prosthesis. In fact, this last test was not well supported by the PLA prototype due to the presence of a barrier for the mobile bearing, figure 8.3. So to overcome this issue new support for the Tibial part was designed without the barrier as shown in figure 8.4.

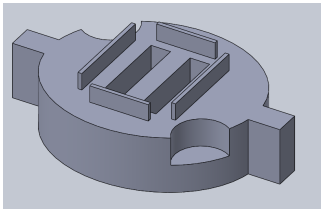

Figure 8.3: Tibial support with containing walls for the mobile bearing

Finally, pressure maps can be observed in the I-Scan GUI both in 3D and 2D, as shown in figure 8.5a and 8.5b respectively. However, data were exported for data processing in Matlab.

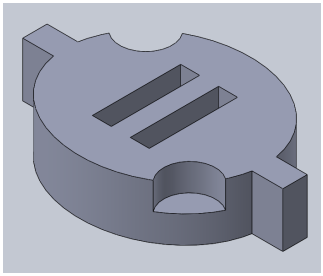

Figure 8.4: Tibial support without containing walls for the mobile bearing

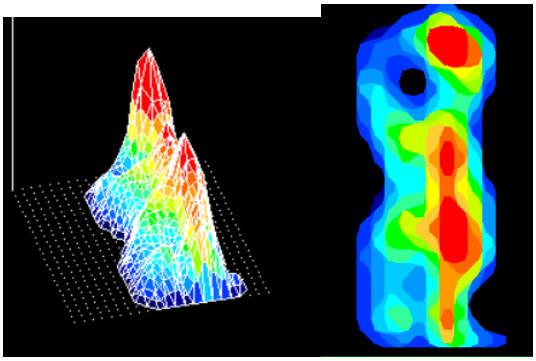

(a) 3D representation (b) 2D representation

Figure 8.5: Pressure map with Tekscan sensor

8.1.1 Sensor fragility

When working with this sensor, a major issue arising during measurement is the sensor's fragility. The sensor was unable to pass multiple cycles during testing without experiencing some damage, as depicted in Figure 8.6. This is due to the high friction between the Tibila and Talar parts during testing, which the sensor is not strong enough to withstand. However, the damage was restricted to 5% of the total rows or columns with not a clear recurrency, with final damage of 1/2 rows over a total of 44 rows.

Additionally, the I-Scan GUI alerts us when the sensor is damaged, and detects if any row of the sensor is no longer active, so examining the force display in the GUI allows us to terminate the test when damage occurs. Furthermore, in order to withstand this problem and to improve the sensor's robustness, scotch tape was added to the sensor's arms and sensitive matrix, allowing it to perform multiple cycles without any damage. On the other hand, we must take into account that the load applied during testing was halved with respect to the real axial load suggested by the ISO standard, so this problem should be resolved for future development.

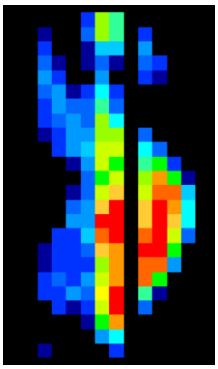

Figure 8.6: I-Scan GUI, display damage in the sensor

8.2 Comparative research

Comparative research is a method of scientific inquiry that aims to identify and analyze the similarities and differences between two or more variables, phenomena, or groups. It is a systematic approach to research that allows researchers to draw conclusions about the relationships between variables by examining how they differ across various contexts or settings.

For this purpose, three types of Tibial components were printed with different angulations with respect to the Anterior/Posterior plane, in particular with the following values 0, 6, and 10 degrees, as shown in figure 8.7. Those pieces were used for different acquisitions of the contact area between the Tibial and Talar components during gait and allowed to perform comparative research of the data obtained. The results will be discussed in the next chapter. Moreover, all the different dispositions

were tested with and without the mobile bearing, which was specifically designed for this purpose, as shown in figure 8.8.

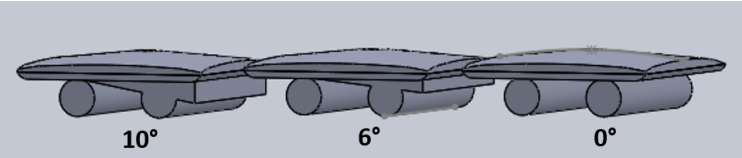

Figure 8.7: Tibial support with different insertion angles, printed in PLA. On the left 10°, in the middle 6°, and on the right 0°

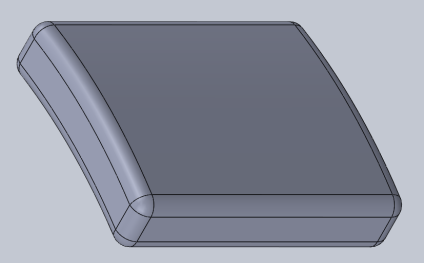

Figure 8.8: Mobile Bearing

The significance of this research lies in its ability to shed light on the changes that occur in the distribution and magnitude of load as a result of variations in the angle at which the prosthesis is implanted relative to the natural axis. Furthermore, the study explores the role of mobile bearings in facilitating load distribution for optimal performance and reduced pressure on both sections of the prosthesis.

8.2.1 Contact area and Force data extraction, evaluation and visualization

Using the Tekscan pressure sensor and the GUI from Tekscan I-Scan 7.60, Area contact data were calculated.

Just looking at the GUI, figure 8.9, we are able to visualize the 2D and 3D map of the pressure distributed over the sensor, and furthermore, also the Raw Sum of the forces, this last data can be used after calibration of the sensor in order to have also an estimation of the Force applied by the Axial motor to the PLA prosthesis. Unfortunately, is difficult for the I-Scan GUI to have a proper comparison of the data obtained with different configurations of the PLA prototype. So in order to proceed in this direction a Matlab code was written to manage the Excel ASCII file that can be exported directly from the GUI.

Basically, this code is able to construct a three-dimensional matrix that contains one matrix representing a 3D pressure map for each frame of the signal, figure 8.10. Where one matrix is composed of the two-dimensional pressure map detected by the sensor at that instant in time. After creating this matrix, the contact area is

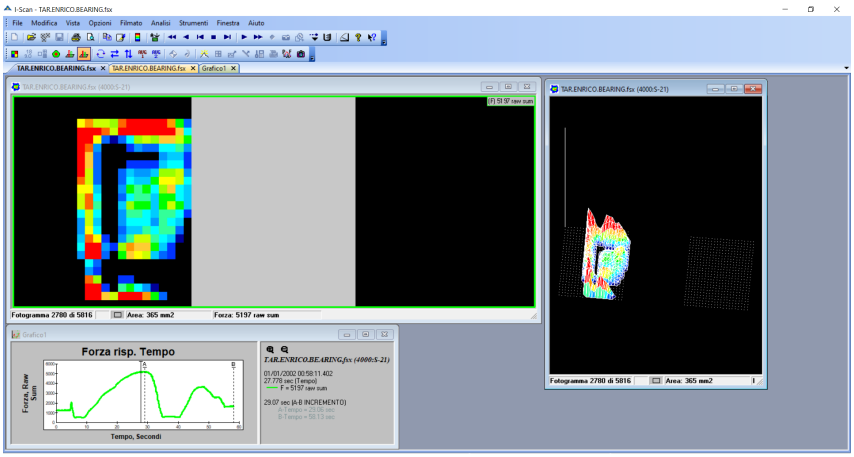

Figure 8.9: I-Scan GUI, Data visualization

calculated for each instant of time. Moreover, the position of the Center of Force in time can be exported from the ASCII file, but this data were not taken into account.

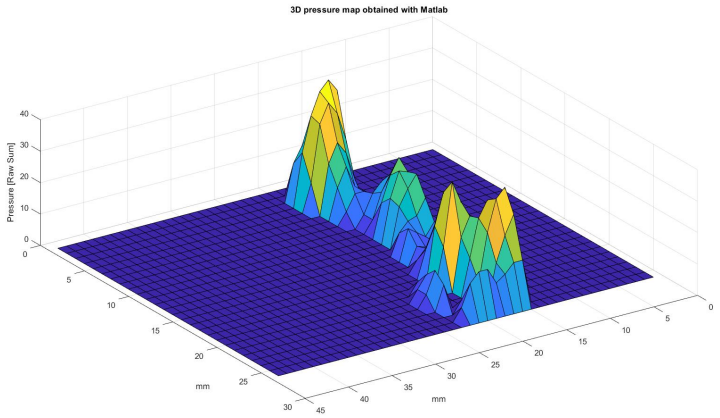

Figure 8.10: 3D surface plot

Chapter 9

Result and discussion

The upcoming chapter will present the outcomes of the C++ application, motor calibration, comparative research, and repeatability testing, which have been conducted to gather valuable data on the performance of the PLA ankle prosthesis prototype and the functionalities attained by the robot.

Specifically, these tests enable the evaluation of the robot's precision, as well as the pressure and contact area data between the Tibial and Talar components, and the robot's consistency.

Accuracy, precision, and consistency were fundamental characteristics to achieve in order to replicate the natural movement of the ankle during different motor tasks, such as walking, running, jumping, or climbing. However, in this thesis, only walking was analyzed, but for future development, further movement can be analyzed by defining the proper position tables.

9.1 Robot synchronization

The first purpose of this thesis was to achieve synchronization between the four motors that compose the robotic simulator. The latter was achieved by the development of a C++ application able to deliver commands to all the motors simultaneously and with great precision, allowing respect to the ISO standard path for Plantar/Dorsiflexion, Internal/External rotation, Anterior/Posterior displacement, and Axial load.

The commands delivered by the C++ application follow the gait cycle path specified in the position tables, created following the ISO standard for all four movements. This was done in order to have a standard test of the ankle prosthesis, but those data can be even acquired directly from the patient using an optoelectronic system to have a personalized test of the prosthesis. Furthermore, the C++ application allows also testing both ankle and knee prostheses under different conditions, for example for running or climbing, but new position tables must be created. In fact, the robot at first utilized for testing knee prostheses was converted in order to test ankle prostheses by previous works, due to the similarity in the movements during gait between the ankle and the knee.

Moreover, this application is functional but still can be implemented with other functionalities helping to automatize the process for example the creation of the

position matrix is still for some parts manual, so that could be a starting point for future development.

9.2 Motors calibration

Motors calibration is crucial for understanding the real performances of each motor and evaluating their accuracy during the simulation. In fact, each degree of freedom must be calibrated in order to understand the differences in movement between the corresponding command and the real movement.

Recordings of the single motor during the simulation and export of those data outside the Motive GUI, figure 9.1, for processing purposes were done. This was performed by selecting one movement at a time from the C++ application, enabling the movement of a single motor, that must change for each record in order to test all four degrees of freedom. Then differences in displacement between the actual movement and the standard table were measured.

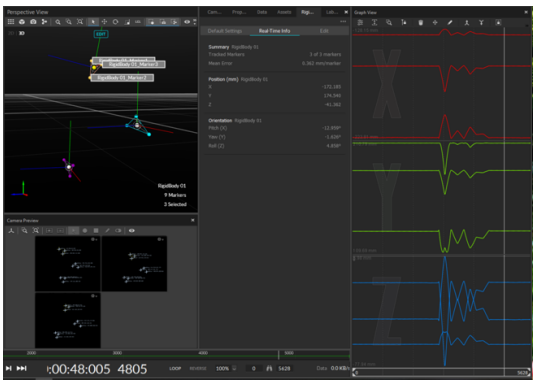

Figure 9.1: Motive GUI, Rigid bodies trajectory reconstruction.

Starting from the Plantar/Dorsiflextion movement, in figure 9.2 the movement is reported with the 95th percentile variability band obtained calculating the standard deviation from the motor movement's error with respect to the ISO standard specification.

For this acquisition 3 marker supports were used with 3 markers each, and the movement was calculated taking into account the rotation of the marker support placed in the axis of rotation of the Plantar/Dorsifexion motor.

In order to calculate the error and the standard deviation, the ISO standard was resampled with a higher sampling frequency, with "polyfit" Matlab function, in order to match the number of samples acquired during calibration.

In this case, for calculating the polynomial curve that best fits the ISO standard a 21° order polynomial was used.

Unfortunately, this method wasn't enough precise to accurately fit the ISO curve so another curve was obtained directly by fitting the ISO curve from the Matlab

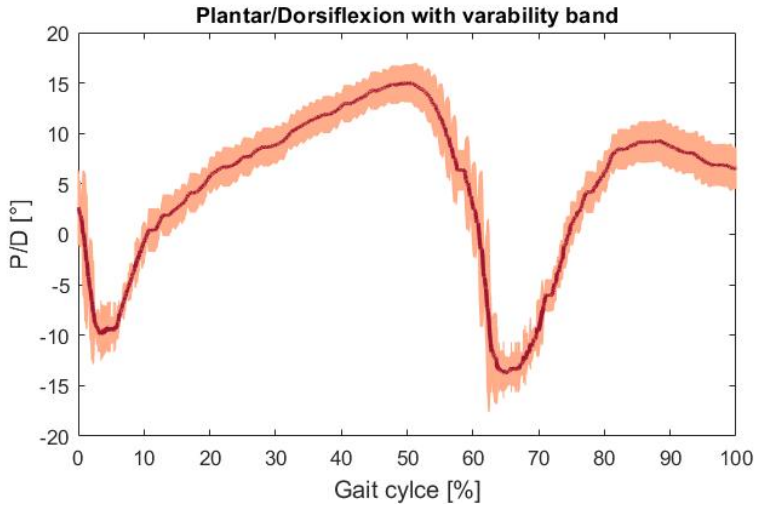

Figure 9.2: Calibration of Plantar/Dorsiflexion motor. The graph report in red the mean value of Plantar/Dorsiflexion obtained during multiple gait cycle and in light red the 95th percentile confidence band obtained from the standard deviation during calibration.

graph, with a tool called "shape-preserving interpolation" from Basic fitting.

After obtaining the resampling of the ISO standard, the error and the standard deviation were calculated. Obtaining the graph in figure 9.2 and figure 9.3, that report the mean movement of the P/D motor during the simulation with the respective variability band, and the mean error with the variability band.

From these two graphs in particular from the second, we can observe how the P/D motor is following the Plantar/Dorsiflexion movement quite closely in almost the majority of the gait with a mean error of -0.3° +/- 2°, while near the 60 % of the gait cycle the motor get a rapid increase of both the error and the standard deviation, reaching a peak of -7.16° +/- 4.67°.

That phase corresponds to the initial part of the swing phase where the foot is detached from the ground and reaches the maximum range of motion of 30°, but still, this does not justify the stiff increment of the error in this phase.

Moreover, this stiff increase can be yielded both by the performance of the robot and also by an error in the tracking system utilized, suggesting that further investigation is needed to better classify the problem.

Observing the overall trend of the error, of course, by excluding the part which reaches the 60 % of the gait cycle where the motor performances have a rapid decrement, the Plantar/Dorsifrexion motor can be considered able to reproduce the movement quite accurately and precisely.

Furthermore, the data were taken directly on the motor without considering the Talar part, but due to the connection, the Talar part follows exactly the movement of the motor.

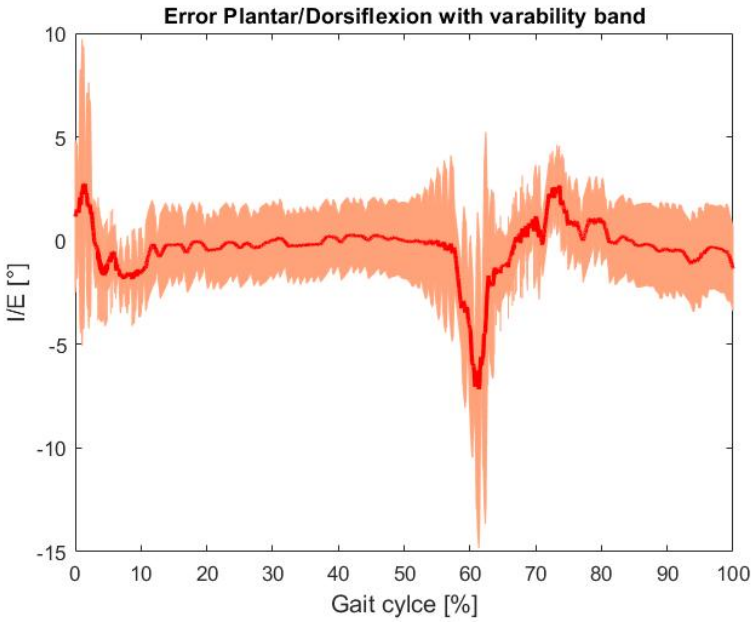

Figure 9.3: Plantar/Dorsiflexion error. In red is the error during calibration of the Plantar/Dorsiflexion motor, calculated with the difference between the real movement and the ISO standard, in light red is the 95th percentile variability band.

The acquisition of Internal/External rotation was performed by calculating the rotation around the axis of rotation of the Internal/External rotation motor.

As previously reported for P/D, also the ISO standard curve of the Internal/External rotation was resampled with a higher frequency, using the "polyfit" function and a polynomial curve of the 30° order, and then the error and the standard deviation were calculated on the basis of the difference between the polynomial curve ad the mean value of the Internal/External rotation performed by the motor over multiple cycles, obtaining the data reported in figure 9.4 and 9.5.

By observing figure 9.5 that reports the error during the calibration, it can be seen that the error is lower than the P/D error and follow the temporal trend of the ISO path. In this case, the range of motion is reduced to 10°, but the error remains lower than 0.6° +/- 0.3°, with a maximum error of 1° +/- 0.4° in the final part of the movement.

Moreover, the variability band reported in figure 9.4, show that the motor is able to replicate the same movement multiple time with low variability with respect to the ISO standard. This trend confirms that the motor has high accuracy, a fundamental characteristic to have during the simulation.

Finally, the I/E motor has achieved both accuracy and precision, suggesting that is optimal for the purpose of the robotic simulator.

The Anterior Posterior displacement where acquired always taking into account

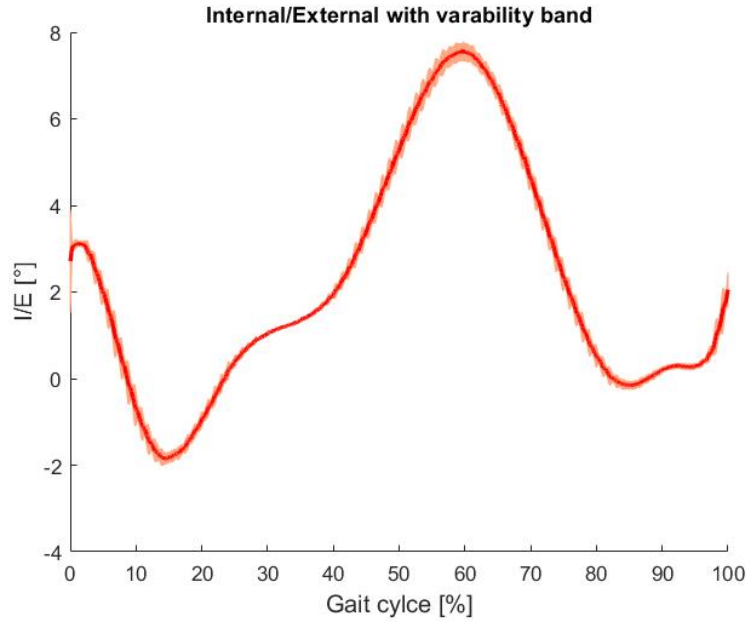

Figure 9.4: Calibration of Internal/External rotation motor. The graph report in red the mean value of Internal/External rotation obtained during multiple gait cycle and in light red the 95th percentile confidence band.

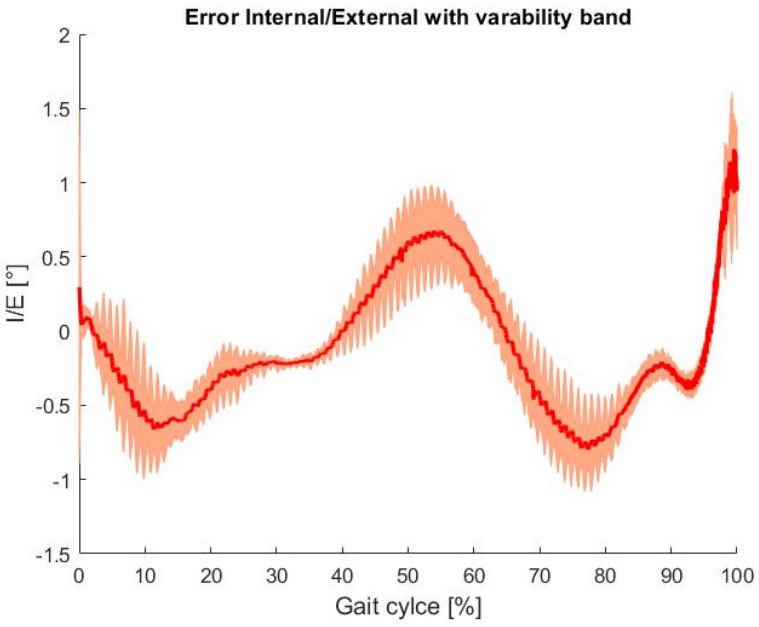

Figure 9.5: Internal/External rotation error. In red is the error during calibration of the Internal/External motor, calculated with the difference between the real movement and the ISO standard, while in light red is the 95th percentile variability band.

the 3 marker dispositions, where two were positioned on the metal frame and the third one on the Anterior/Posterior plate, and the movement was calculated with the difference between the position along X axis of the rigid body on the metal frame and the one positioned in the A/P plate.

For the estimation of the error, the ISO path for the A/P was resampled with a polynomial curve of 21°, and the difference between the mean value and the ISO was calculated, figure 9.6. Moreover, the standard deviation was calculated, obtaining the graph in figure 9.7.

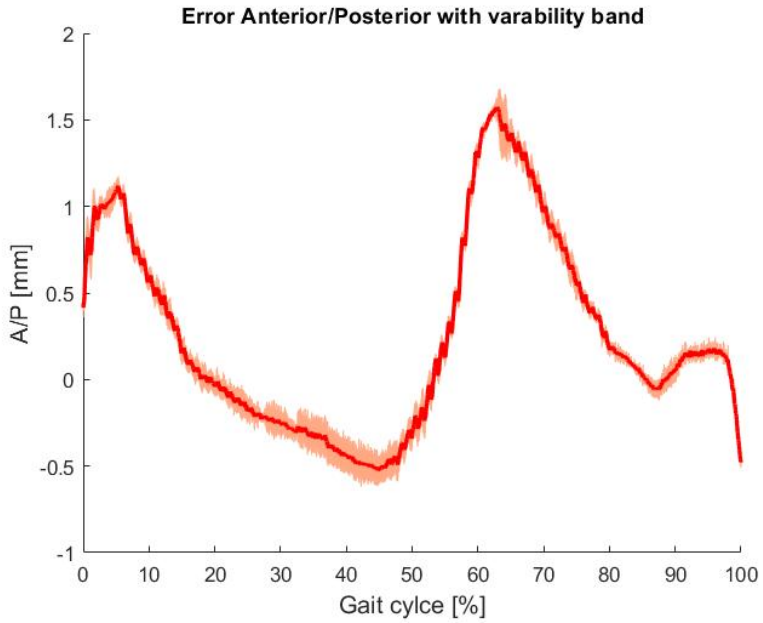

Figure 9.6: Anterior Posterior displacement error. In red is the error during calibration of the Anterior Posterior displacement motor, calculated with the difference between the real movement and the ISO standard, and in light red is the 95th percentile variability band.

The A/P motor shows a low value of standard deviation, as reported in figure 9.7, suggesting that the motor is able to perform the same path multiple times without deviating from the mean value.

On the other hand, the error reported in figure 9.6, shows a recurrent trend where the error increase when the A/P displacement reaches the maximum range. Particularly in the initial part from 0 to 10 % of the gait cycle, with a maximum value of 1 mm +/- 0.15 mm, and around the 60 % of the gait cycle, with a peak of 1.6 mm +/- 0.1 mm. On the basis of those error data and considering the limited range of motion of the A/P displacement of around 5 mm, the A/P motor achieves only precision due to low standard deviation but low accuracy yield by the high values of error.

Moreover, looking at figure 9.6, the error trend suggests that the motor seams accentuate the A/P displacement in the part in which the A/P reaches both a

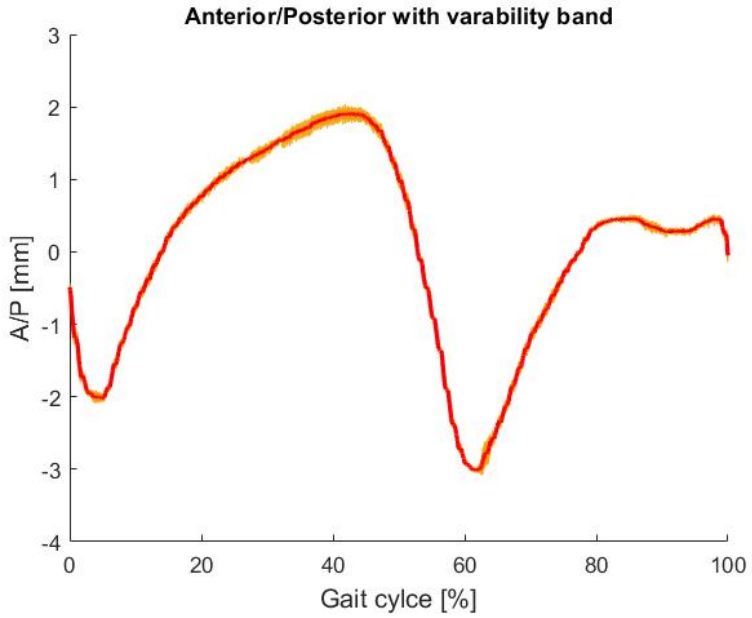

Figure 9.7: Calibration of Anterior/Posterior displacement motor. The graph report in red the mean value of Anterior/Posterior displacement obtained during multiple gait cycle and in light red the 95th percentile confidence band obtained from the standard deviation during calibration.

minimum and a maximum. Upon the latter consideration, a recalculation of the NEMA mm/step ratio (0.00158) reported in table 4.2 is necessary.

Finally, for what concern the axial motor, the calibration was not performed, but the motor was controlled considering the graph for A8 (reported in the datasheet of the motor) in figure 9.8 that reports the load in newton [N] in relation to the current applied [A]. On the basis of this graph, a proportion was calculated in order to control the motor directly applying the exact amount of current to have the right load delivered.

Looking at the result obtained from the motor calibration, the robotic simulator achieves low variability for Internal/External rotation and Anterior/Posterior displacement, while for Plantar/Dorsiflexion the variability increase. Furthermore, the error trend yield that the motors increase their error when the range of motion is maximum, with particular evidence in the P/D and A/P motors, while for the I/E motor, the error remains around the mean value.

These data suggest performing a further investigation into motors to better understand their accuracy and precision, in particular on the P/D and A/P motors.

Moreover, motor calibration results report clearly that the optoelectronic system used for motion capture is extremely functional for the purpose, due to the fact that the movement was detected with minimal error.

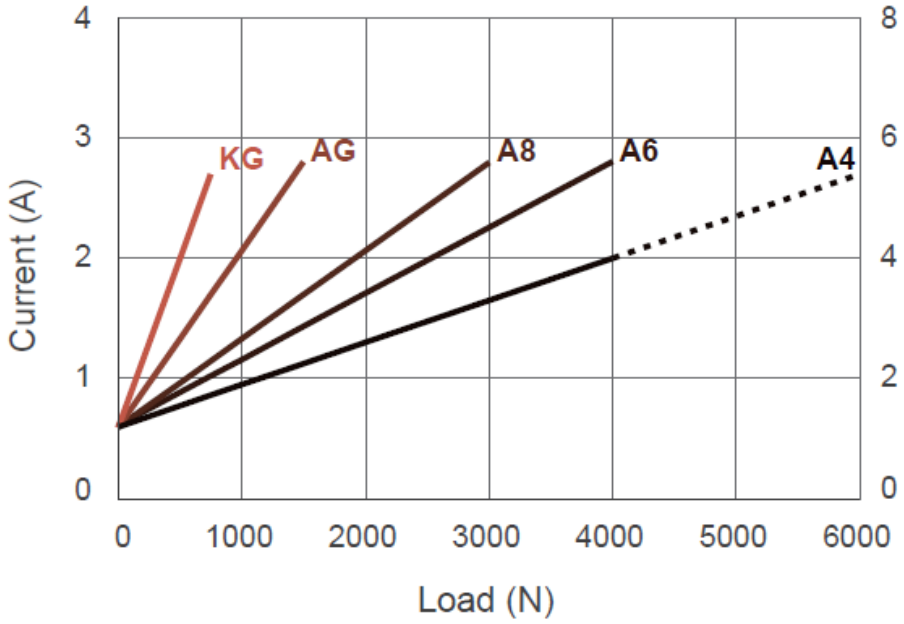

Figure 9.8: Axial motor calibration. The proportion used for control of the axial motor was calculated on the basis of this graph, in particular, our motor follows the linear relationship named A8.

9.3 Comparative research

Comparative research was made between 10 configurations of the Tibial part of the prosthesis, which are the following:

- Zero Degree, with mobile bearing or not.
- Six Degree with respect to the Anterior/Posterior plane, with mobile bearing or not, and both Eversion and Inversion.
- Ten Degree with respect to the Anterior/Posterior plane, with mobile bearing or not, and both Eversion and Inversion.

This research was done in order to estimate the changes in the contact area between the Talar part and the Tibial part of the TAR. The latter is a fundamental character that influences the failure rate of the prosthesis, in fact, taking into account the anatomy of the ankle the area of contact increases during gait reaching the maximum when the load applied is maximum in order to better distribute the load [22].

The second purpose of this research was to prove the differences in functionality between the use of a mobile bearing and the use of a fixed bearing. Looking at the literature, there are no articles speaking directly about the typical values of contact area for the TAR, but looking at the anatomical behavior of the cartilage during load is clear how the use of a mobile bearing should help the prosthesis to replicate the ankle movement. Furthermore, analysis of the knee prosthesis is strongly present in

the literature and for this type of prosthesis, the use of a mobile bearing is strongly recommended for a better outcome [36], supporting the opinion previously stated.

The graph shown in figure 9.9 displays the area of contact value when the Tibial part is parallel to the ground plane. The graph demonstrates how the presence of the mobile bearing is crucial in achieving a more even distribution of the load exerted by the Talar part during gait. There is a notable difference of around 45 mm^2 in the maximum contact area, which corresponds to the peak of axial force observed during the test, corresponding to the 40 % of the gait cycle. This pattern is consistently present across all 10 different configurations, indicating that a well-designed mobile bearing can increase the contact area and reduce the overload of critical bone components.

Additionally, the graph's trajectory is similar in both configurations and follows the Plantar and Dorsiflexion path specified by the ISO. This behavior is led from the path of P/D because the maximum of P/D, between 60 % and 70 % of the gait cycle, corresponds to the minimum contact between the two parts of the prosthesis, leading to a decrement in the contact area.

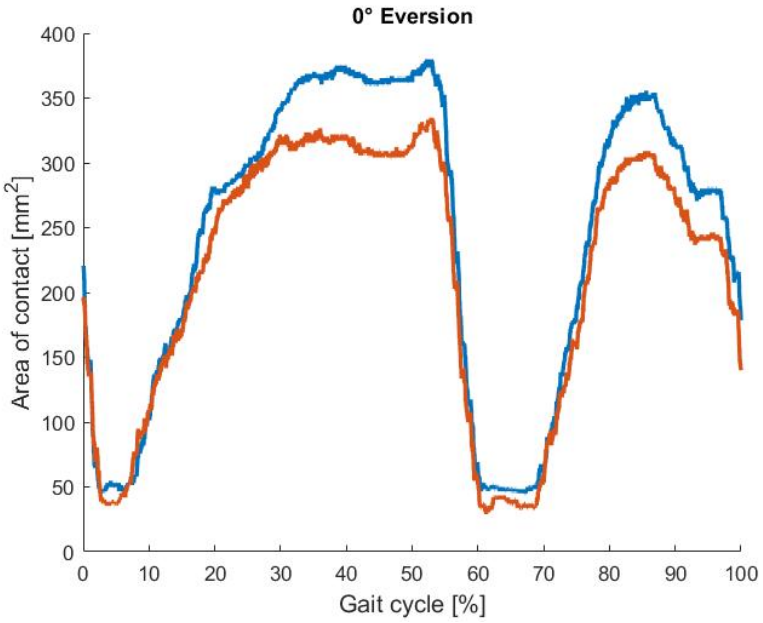

Figure 9.9: Area of contact calculated with the pressure sensor considering 0° of Eversion. The blue curve represents the Area of contact considering the mobile bearing, while the Orange line represents the configuration without the mobile bearing

By analyzing figures 9.10 and 9.11, which illustrate the area value in the 6 degree configurations, it can be observed that the presence of the mobile bearing continues to play a crucial role in load distribution, similar to what was seen in the 0 degree configuration. Specifically, there is a noticeable decrease in the contact area, with a reduction of 111.06 mm^2 and 131.99 mm^2 for the Inversion and Eversion, respectively,

configurations during the peak of force while testing.

In both of these two configurations of 6 degrees Inversion and Eversion, the behavior of the P/D is respected with a minimum contact area during the initial part of the swing phase. Moreover, due to the presence of mobile baring in the test performed in 6 degree Eversion is notable a rapid decrease in the contact area around the 40 % of the gait, this behavior can be led to a lateral movement of the mobile bearing during the movement due to the inclination of the Talar part. However, the latter movement is limited in real situations due to the presence of ligaments and bones that surround the prosthesis, so this stiff decreases in the contact area should be limited or not present.

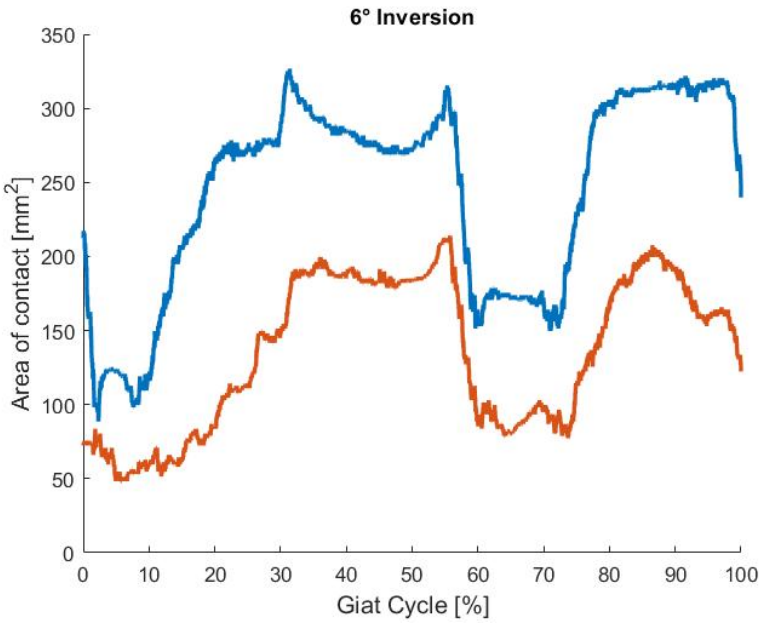

Figure 9.10: Area of contact calculated with the pressure sensor considering 6 degrees of Inversion. The blue curve represents the Area of contact considering the mobile bearing, while the Orange line represents the configuration without the mobile bearing

Finally, in Figures 9.12 and 9.13, a similar trend is observed, with a decrease in the contact area of 33.80 mm^2 and 87.92 mm^2 for the Inversion and Eversion configurations during the peak of force while testing, respectively. However, there is a deviation from the expected movement path in the Eversion configuration, while the Inversion configuration follows the normal trajectory. This anomaly requires further investigation since the observed values may be affected by the material weakness of the 3D-printed components used in the test and also by the displacement during the simulation of the mobile bearing due to the increased abnormality in the position angle. These findings suggest the importance of using high-quality materials for 3D printing prosthetic components to ensure accurate and reliable results.

Upon a thorough analysis of the aforementioned graphs, it becomes evident that

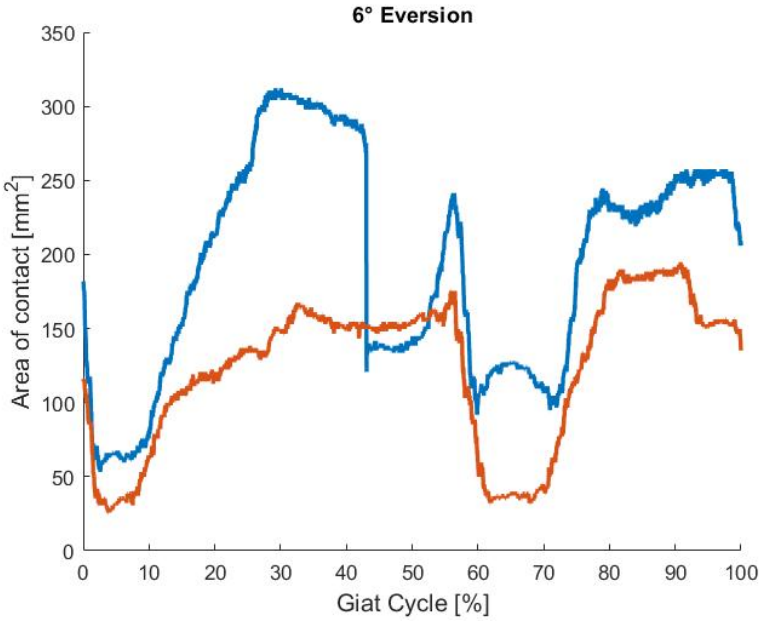

Figure 9.11: Area of contact calculated with the pressure sensor considering 6 degrees of Eversion. The blue curve represents the Area of contact considering the mobile bearing, while the Orange line represents the configuration without the mobile bearing

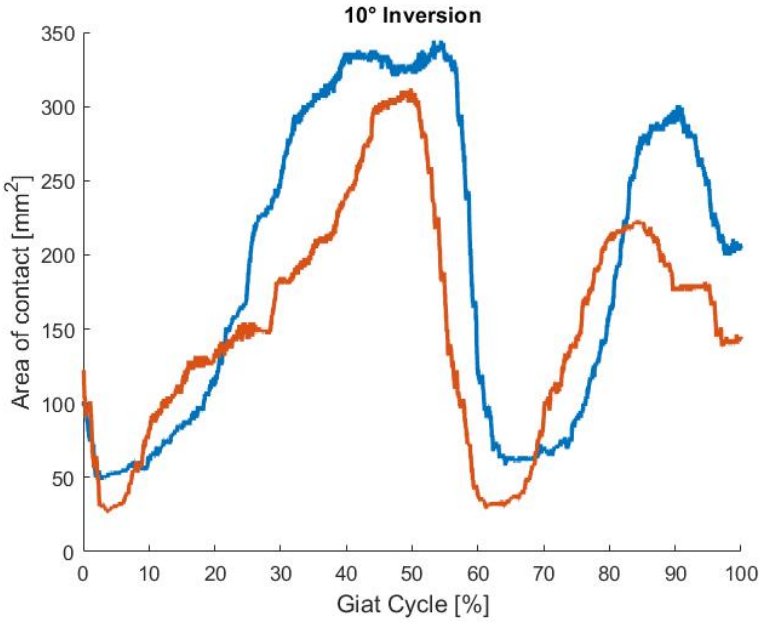

Figure 9.12: Area of contact calculated with the pressure sensor considering 10 degrees of Inversion. The blue curve represents the Area of contact considering the mobile bearing, while the Red line represents the configuration without the mobile bearing

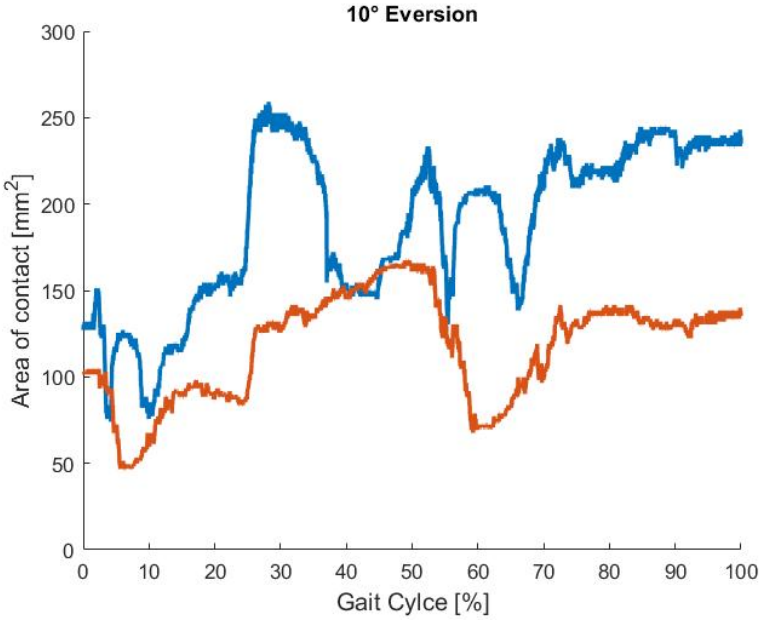

Figure 9.13: Area of contact calculated with the pressure sensor considering 10 degrees of Eversion. The blue curve represents the Area of contact considering the mobile bearing, while the Red line represents the configuration without the mobile bearing

a consistent reduction in the contact area is observed when transitioning between various configurations. The most favorable outcomes are achieved when the prosthesis is implanted at a 0-degree angle with respect to the Anterior/Posterior plane, in parallel with the ground, and when a mobile bearing is employed. These findings underscore the importance of precise positioning of the prosthesis during implantation and highlight the benefits of utilizing mobile bearings to enhance the performance and longevity of the prosthetic joint.

In fact, the ankle prosthesis positioned with a 0-degree angle with respect to the Transverse plane has better performances in terms of area of contact and consequently for the distribution of the load during movement.

However, during surgery, alignment of the prosthesis is not easy due to visibility factors so a computer-assisted or virtual reality system can be developed to access a better visualization of the axis and a better positioning of the prosthesis, as already append for knee prosthesis [37].

9.4 Repeatability test

Repeatability tests are an essential component of scientific research and quality assurance, as they provide a means of evaluating the consistency and reliability of measurements, instruments, and procedures. The purpose of a repeatability test is to assess the extent to which a measurement or experimental result can be

reproduced under identical conditions, thereby providing an objective assessment of its accuracy and precision. Repeatability tests are particularly relevant in fields such as engineering where precise and consistent measurements are critical to advancing scientific knowledge and ensuring the safety and efficacy of products and processes.

In fact, for our purpose in order to fully respect the ISO standard for the wear test of the prosthesis, the robot should be able to replicate the same gait cycle a hundred times or more. For this reason, a repeatability test was needed, in order to evaluate if the robot is consistent.

For this test, only one of the previous 10 configurations is analyzed, and in particular, the one with the higher result concerning contact area in the previous test so the 0-degree Eversion with mobile bearing. Moreover, for this test, the robot performed 8 cycles of gait in sequence, and the data are always acquired with the pressure sensor previously described.

Acquired data were analyzed with a first visual inspection and the first cycle was discharged by default because it presents some variations due to the initial settling of the motors, as shown in figure 9.14.

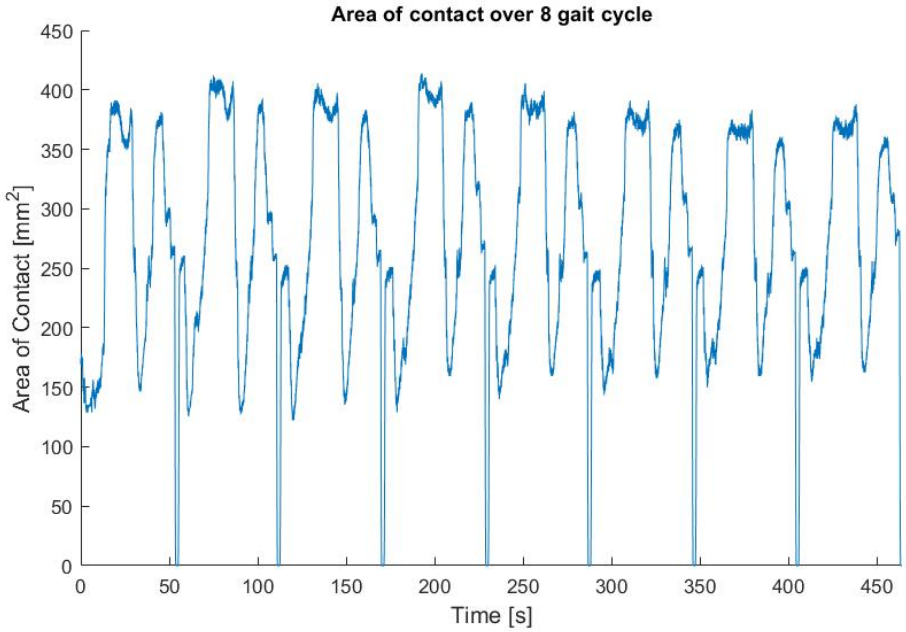

Figure 9.14: Area of contact over the repeatability test

After this first inspection, data from the different cycles were divided. Further manipulation of the data is needed for achieving a perfect time alignment of all the graphs, allowing us to obtain what is shown in figure 9.15. Moreover, to obtain this graph a point of congruence was taken into account and all the graphs were shifted to the left or right to achieve higher congruence.

Starting from data shown in figure 9.15, the mean value, error, and standard deviation were calculated, obtaining the graph reported in figure 9.16. The latter

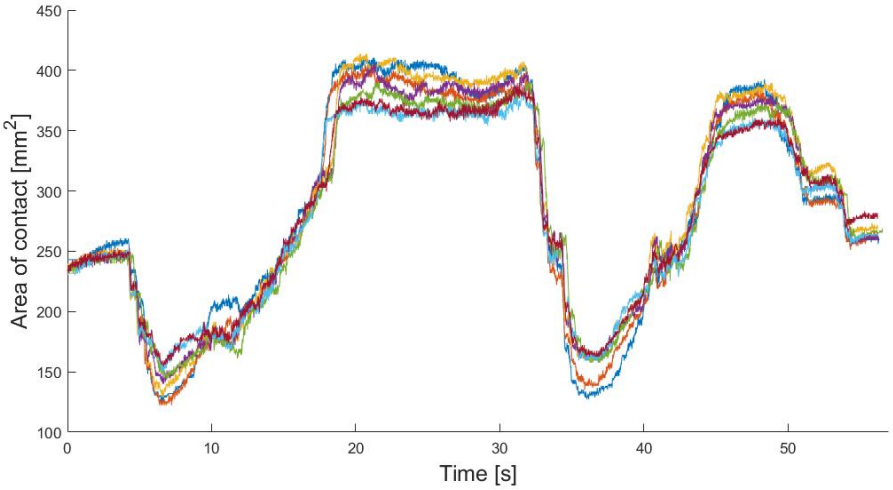

Figure 9.15: Area of contact over repeatability test with overlapped signals and aligned graphs

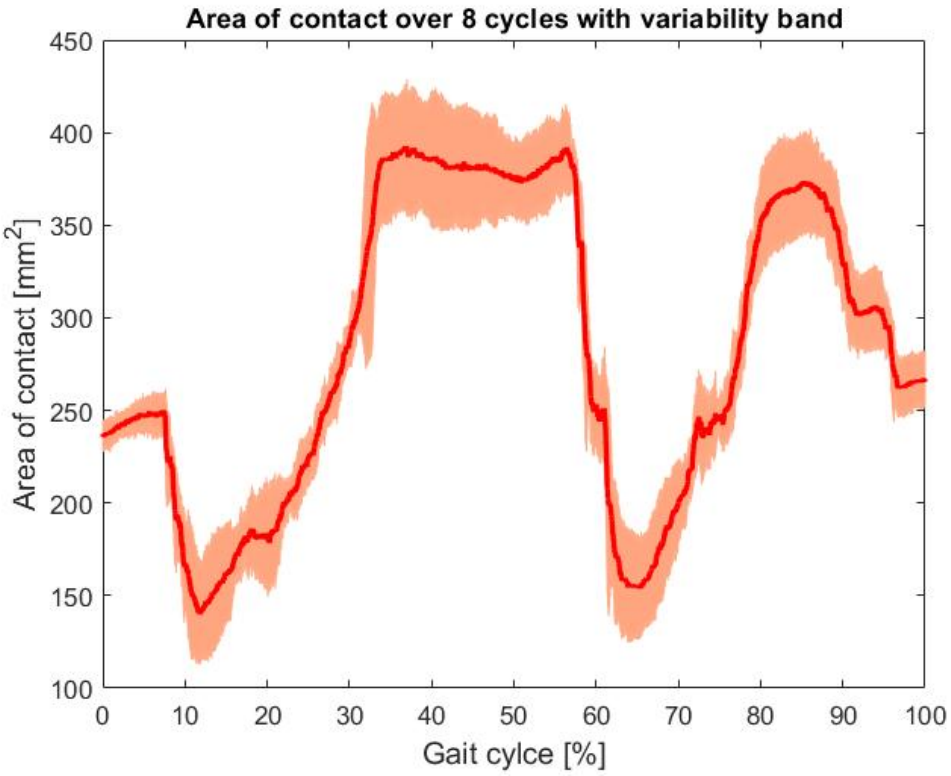

Figure 9.16: Area of contact over repeatability test with variability bands in light red and mean value in red

shows how the robotic simulator is able to reproduce the same pattern of contact area over different simulations, increasing the variability in the part in which the load applied is maximum or minimum, in fact during ascending or descending phases the standard deviation is reduced to the minimum.

Furthermore, this result shows that the robot has low variability during ascending and descending parts, while in phases where the load is maximum or minimum, the variability of the load applied increases, this could be led both by the fact that the Talar part is not fixed to the Z axis during the simulation and also by the fact that the mobile bearing could move during the simulation causing a different distribution of the contact area.

Finally, the repeatability test graph, figure 9.16, yields another important information that must be taken into account for a better understanding of the behavior of the mobile bearing. In particular, during the phase in which the axial load is maximum the variability band increase, reaching a value of +/- 50 mm^2.

The latter behavior, due to a not marked distinction between the contact area with the mobile bearing and without it, could lead to the conclusion that during the normal use of the prosthesis, the use of the mobile bearing doesn't lead always to a better distribution of the load between the Talar and Tibial part. However, the contact area with the mobile bearing remains higher, so should be considered anyways as a better solution with respect to the fixed bearing configuration.

9.5 Future improvements

9.5.1 Mechanical improvement

Despite mechanical issues, solutions were developed, and the robot performed well during testing. However, two of them should be further developed, in particular, it was noted that the axial motor continued to have displacement along the Z axis during testing, and the Plantar/Dorsiflexion joint was not able to withstand the torque exhorted by the axial motor leading to an angular displacement during the simulation.

To address the first issue, several solutions have been proposed, including the use of a toothed pulley or a direct connection between the axial motor and the internal/external rotation motor. Where the first solution requires the realization of two metal-toothed pulleys and the purchase of a toothed belt, while the latter solution would involve modifying the robot's mechanical structure, positioning the axial motor above the internal/external rotation motor, and creating new metal supports, figure 9.17. However, this direct connection would prevent problems related to the tensioning system and wear and tear of the transmission belt.

While, for the second issue, a proper modification of the P/D joint can solve the problem, for example by introducing an interlocking in the connection between the P/D joint and the Talar part, allowing the screw that keeps contact between the

Talar part and the motor, avoiding sliding during the test. However, for the scope of this thesis, the problem was solved by scaling the force applied to the prosthesis, as reported in the previous chapter.

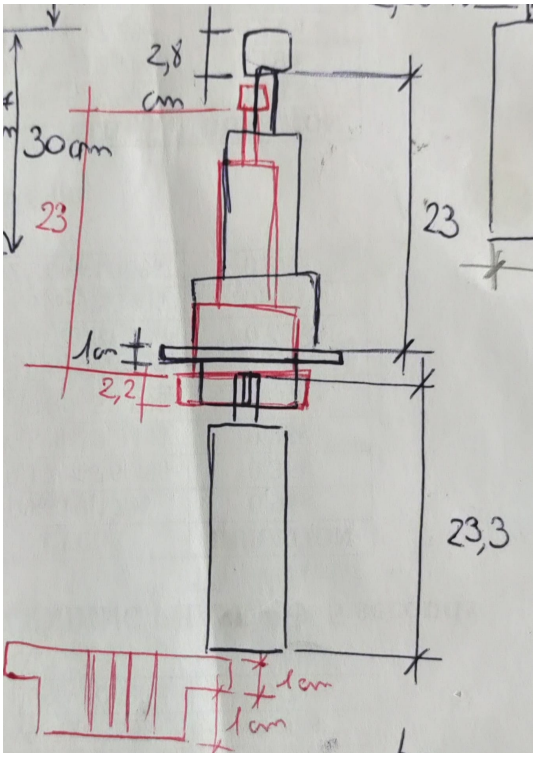

Figure 9.17: Raw Drawing for the direct connection

9.5.2 Pressure sensor improvement

For what concern the pressure sensor Tekscan 4000 utilized during tests, allows measuring with high accuracy the behavior of the area of contact and that of the pressure distribution which are two fundamental parameters to take into account. However, during measurement, the calibration was not performed due to difficulty in the process, and the requirement of specific instrumentation for calibration. Besides that, the sensor is still able to give a raw estimation of the force which can still be utilized after calibration to have the measurement of the force applied. Moreover, what concerns sensor fragility can be solved by applying a protective layer in the sensor itself as was performed during this thesis or even thinking to realize a PLA 3D cage for containing the sensor and inserting that between the Tibial and Talar parts.

Chapter 10

Conclusion

Throughout the course of this project, the functionalities of the robotic simulator were substantially increased, considering that at the starting point, the robot was just a metal structure and four motors that were not able to move in synchro or move at all, as in the case of the axial motor. In fact, at the outset of the project, the robot was plagued by several electrical and mechanical issues that required attention. However many of these issues were successfully resolved, and the remaining part needs to be solved for future development.

Initially, the first step in addressing the robot's issues was to resume the previous code and improve it. This was essential in ensuring that the robot was able to operate effectively and efficiently. This was done by developing a C++ application able to deliver commands to the robot and move all the motors in synchro following the paths specified by the ISO standard for the gait cycle.

Next, the electrical circuit responsible for controlling the axial motor was identified as damaged, and efforts were made to repair it.

Additionally, the mechanical issues plaguing the robot were identified and addressed, as detailed in previous paragraphs. However, some of them still need to be solved but a proper solution was proposed in the previous chapter.

Following the initial phase, the EZI-Motion controlled motors underwent a calibration process through an optoelectronic system to evaluate their ability to accurately and precisely execute commands issued by the application. However, the axial motor, being force-driven, did not require such calibration but was controlled on the basis of a proportion yield by the relationship between the newton exerted by the motor and the current delivered to it.

The motor calibration process was carried out one motor at a time using an optoelectronic system to ensure the motors' accuracy and precision. From this test, the motors show different performances, in particular, only one motor achieves both accuracy and precision with low error and variability band that is the I/E motor. The P/D motor shows good accuracy and mediocre precision excluding the initial phase of the swing, which has a rapid increase in both error and standard deviation leading to a decrement in motor accuracy and precision. For concern the A/P motor, the variability is low but the error is quite high considering the limited range of motion of the A/P displacement.

On the basis of this consideration, the motor's performance should be increased in order to achieve both accuracy and precision for all the motors, by adding other feedback mechanisms for example.

After calibration, comparative research and repeatability test were performed.

Starting from comparative research, the result suggests that two factors can influence the performance of the TAR. First, the position angle at which the prosthesis is positioned influences the functionalities, in particular, the more the angle differs from the neutral position, 0° Eversion, the more the contact area decrease, leading to an overloading of the bones during movement and causing an early failure of the prosthesis. Second, the use of the mobile bearing slightly increases the contact area and so the load distribution between the Talar part and the Tibial part, allowing to reduce the overload during the movements of the ankle.

The repeatability test suggests that the robot is able to replicate the same load during multiple gait cycles, with the variability band that increases its value, especially in the phases in which the load is maximum or minimum. Suggesting that the contact area is influenced by the load applied and also that during those phases the mobile bearing is able to move and consequently change the contact area value.

Overall, through careful attention to detail and a concerted effort to address the robot's initial electrical and mechanical issues, the robot's functionalities were greatly increased.

The robotic simulator has now all the characteristics to be implemented for a wear test of an ankle prosthesis. Unfortunately, this result can't be compared with other robotic simulators due to the absence of literature concerning this argument, especially in reporting the result of robot performances.

Upon examination of the PLA prototype following testing, it became apparent that the mobile bearing, in particular, did not possess the mechanical resistance to fulfill the test's intended purpose, leading to a failure of the material over testing. However, this does not mean a setback in the development process. Instead, it indicates that further enhancements to the material should be explored to improve its resistance and enable the robot to execute multiple tests without material failure. In the future, introducing a fully-realized prosthesis with enhanced material properties will facilitate achieving the desired results. Thus, while the current prototype was unable to meet the testing criteria, it has provided valuable insight into the areas of improvement necessary for the development of a successful prosthesis.

Finally, ISO 22622:2019 provides robotic guidance on how to carry out a wear test on the prosthesis, but this outcome is outside the purview of this thesis since carrying out a wear test requires thousands of cycles in order to understand how the prosthesis responds in actual usage. However, despite the unresolved mechanical problems and the reduction in force that was applied, looking at the overall performance of the robotic simulator during the testing of the ankle prosthesis, it's clear that the robot presents all the technical characteristics to perform wear tests and also further experiments on the prototyping of a new prosthesis and the improvement of that,

leading to improve the prototyping method.

Bibliography

[1] Davide Edoardo Bonasia, Federico Dettoni, John E Femino, Phinit Phisitkul, Margherita Germano, and Annunziato Amendola. Total ankle replacement: why, when and how? *The Iowa orthopaedic journal*, 30:119, 2010.

[2] Alexander VAN, Saskia VAN HEUVEL, and Greta Dereymaeker. Total ankle replacement design evolution and results. *Acta Orthopædica Belgica*, 76:150–161, 2010.

[3] A Bianchi, N Martinelli, E Sartorelli, and F Malerba. The bologna–oxford total ankle replacement: a mid-term follow-up study. *The Journal of Bone and Joint Surgery. British volume*, 94(6):793–798, 2012.

[4] Tassos Natsakis, Josefien Burg, Greta Dereymaeker, Ilse Jonkers, and Jos Vander Sloten. Foot–ankle simulators: A tool to advance biomechanical understanding of a complex anatomical structure. *Proceedings of the Institution of Mechanical Engineers, Part H: Journal of Engineering in Medicine*, 230(5):440–449, 2016.

[5] https://www.earthslab.com/anatomy/ankle-joint-talocrural joint/. *Ankle joint.*

[6] https://teachmeanatomy.info/lower limb/joints/subtalar/. *Subtalr joint.*

[7] https://www.lecturio.com/concepts/ankle joint/. *X-ray ankle.*

[8] Richard Drake, A Wayne Vogl, Adam WM Mitchell, Richard Tibbitts, and Paul Richardson. *Gray's Atlas of Anatomy E-Book.* Elsevier Health Sciences, 2020.

[9] Marian G Alvarez-Perez, Mario A Garcia-Murillo, and J Jesús Cervantes-Sánchez. Robot-assisted ankle rehabilitation: A review. *Disability and Rehabilitation: Assistive Technology*, 15(4):394–408, 2020.

[10] https://www.verywellhealth.com/ankle-anatomy-and-physiology 3119098. *Ankle loads.*

[11] Rahul Kakkar and MS Siddique. Stresses in the ankle joint and total ankle replacement design. *Foot and Ankle Surgery*, 17(2):58–63, 2011.

[12] https://www.hmpgloballearningnetwork.com/site/podiatry/current-and-emerging-insights-total-ankle replacement. *X-ray TAR.*

[13] Junitha M Michael, Ashkahn Golshani, Shawn Gargac, and Tarun Goswami. Biomechanics of the ankle joint and clinical outcomes of total ankle replacement. *Journal of the mechanical behavior of biomedical materials*, 1(4):276–294, 2008.

[14] Samantha Bee Lian Low, Matthew Kim, Toby Smith, David Loveday, Alex MacGregor, and Andoni P Toms. The reliability of radiographic measures of total ankle replacement position: an analysis from the oars cohort. *Skeletal Radiology*, 50:1411–1417, 2021.

[15] Josefien Burg, Koen Peeters, Tassos Natsakis, Greta Dereymaeker, Jos Vander Sloten, and Ilse Jonkers. In vitro analysis of muscle activity illustrates mediolateral decoupling of hind and mid foot bone motion. *Gait & posture*, 38(1):56–61, 2013.

[16] Taylor P Stauffer, Billy I Kim, Caitlin Grant, Samuel B Adams, and Albert T Anastasio. Robotic technology in foot and ankle surgery: A comprehensive review. *Sensors*, 23(2):686, 2023.

[17] Beat Hintermann and Victor Valderrabano. Total ankle replacement. *Foot and ankle clinics*, 8(2):375–405, 2003.

[18] Claire L Brockett and Graham J Chapman. Biomechanics of the ankle. *Orthopaedics and trauma*, 30(3):232–238, 2016.

[19] https://www.kenhub.com/en/library/anatomy/transverse-tarsal joint. *Transverse Tarsal Joint*.

[20] https://www.physio pedia.com/Foot_and_Ankle_Structure_and_Function. *Ankle structure*.

[21] Junitha M. Michael, Ashkahn Golshani, Shawn Gargac, and Tarun Goswami. Biomechanics of the ankle joint and clinical outcomes of total ankle replacement. *Journal of the Mechanical Behavior of Biomedical Materials*, 1(4):276–294, 2008.

[22] Mamori Kimizuka, Hisashi Kurosawa, and Toru Fukubayashi. Load-bearing pattern of the ankle joint: contact area and pressure distribution. *Archives of orthopaedic and traumatic surgery*, 96:45–49, 1980.

[23] Jacquelin Perry, Jon R Davids, et al. Gait analysis: normal and pathological function. *Journal of Pediatric Orthopaedics*, 12(6):815, 1992.

[24] David Levine, Jim Richards, and Michael W Whittle. *Whittle's gait analysis*. Elsevier health sciences, 2012.

[25] Lisa M Coester, Charles L Saltzman, John Leupold, and William Pontarelli. Long-term results following ankle arthrodesis for post-traumatic arthritis. *JBJS*, 83(2):219, 2001.

[26] https://www.orthobullets.com/foot-and-ankle/7052/ankle arthrodesis-popup/image/3915. *Arthrodesis*.

[27] Francesco Cenni, Alberto Leardini, Andrea Cheli, Fabio Catani, Claudio Belvedere, Matteo Romagnoli, and Sandro Giannini. Position of the prosthesis components in total ankle replacement and the effect on motion at the replaced joint. *International orthopaedics*, 36:571–578, 2012.

[28] Martinus Richter, Stefan Zech, Ralf Westphal, Yvone Klimesch, and Thomas Gosling. Robotic cadaver testing of a new total ankle prosthesis model (german ankle system). *Foot & ankle international*, 28(12):1276–1286, 2007.

[29] https://thelkin.com/en/products-en-2/special-systems-en/foot-ankle-tester en.html. *Thelkin*.

[30] http://shorewestern.com/Foot.php. *Shorewestern*.

[31] Marie Lobert. Development of a robotic simulator for biomechanical evaluations of total knee arthroplasty. *ULB*, 2020-2021.

[32] Smeesters Tristan. Design and validation of a robot for total ankle replacement (tar) prosthesis analysis. *ULB*, 2021-2022.

[33] SKF. Rolling bearing - skf.

[34] David QK Ng, Chin Tat Lim, Amit K Ramruttun, Ken Jin Tan, Wilson Wang, and Desmond YR Chong. Biomechanical analysis of proximal tibia bone grafting and the effect of the size of osteotomy using a validated finite element model. *Medical & Biological Engineering & Computing*, 57:1823–1832, 2019.

[35] https://www.tekscan.com/sites/default/files/resources/IDL Pressure-Mapping-Sensor-4000-Datasheet_0.pdf. *Teskcan Pressure sensor 4000 data sheet*.

[36] Dongsheng Hao and Junjie Wang. Fixed-bearing vs mobile-bearing prostheses for total knee arthroplasty after approximately 10 years of follow-up: a meta-analysis. *Journal of Orthopaedic Surgery and Research*, 16:1–9, 2021.

[37] Emil G Haritinian and Ashvin L Pimpalnerkar. Computer assisted total knee arthroplasty: does it make a difference? *Maedica*, 8(2):176, 2013.